

Development of a sequential tool, LMDZ-NEMO-med-V1, to conduct global to regional past climate simulation for the Mediterranean basin: An Early Holocene case study

Tristan Vadsaria^{1,3}, Laurent Li², Gilles Ramstein¹ and Jean-Claude Dutay¹

¹Laboratoire des Sciences du Climat et de l'Environnement, CEA-CNRS- Université Paris Saclay, Gif-sur-Yvette, 91191, France

²Laboratoire de Météorologie Dynamique, CNRS-ENS-Ecole Polytechnique- Sorbonne Université, Paris, 75005, France

³Atmosphere and Ocean Research Institute, University of Tokyo, Kashiwanoha, Chiba, Japan

Correspondence to: Tristan Vadsaria (tristan.vadsaria@lscce.ipsl.fr)

Abstract

Recently, major progress has been made in the simulation of the ocean dynamics of the Mediterranean using atmospheric and oceanic models with high spatial resolution. High resolution is essential to accurately capture the synoptic variability required to initiate intermediate and deep-water formation, the engine of the MTC (Mediterranean Thermohaline Circulation). In paleoclimate studies, one major problem with the simulation of regional climate changes is that boundary conditions are not available from observations or data reconstruction to drive high-resolution regional models. One consistent way to advance paleoclimate modelling is to use a comprehensive global to regional approach. However, this approach needs long-term integration to reach equilibrium (hundreds of years), implying enormous computational resources. To tackle this issue, a sequential architecture of a global-regional modelling platform has been developed for the first time and is described in detail in this paper. First of all, the platform is validated for the historical period. It is then used to investigate the climate and in particular, the oceanic circulation, during the Early Holocene. This period was characterised by a large reorganisation of the MTC that strongly affected oxygen supply to the intermediate and deep waters, which ultimately led to an anoxic crisis (called sapropel). Beyond the case study shown here, this platform may be applied to a large number of paleoclimate contexts from the Quaternary to the Pliocene, as long as regional tectonics remain mostly unchanged. For example, the climate responses of the Mediterranean basin during the last interglacial (LIG), the last glacial maximum (LGM) and the Late Pliocene, all present interesting scientific challenges which may be addressed using this numerical platform.

1 Framework of the study

1.1. Introduction

The Mediterranean basin is a key region for the global climate system. It is considered to be a climate “hotspot” (Giorgi, 2006), due to its high sensitivity to global warming. In the past, it has been the seat

36 of important human civilisations, and it continues to play a very important role in international
37 geopolitics with a dense population along its coasts. There is great diversity in the Mediterranean
38 ecosystems, both marine and terrestrial. The Mediterranean region is also rich in paleoclimate records
39 with a variety of proxies. Indeed, this area experienced major changes during the glacial-interglacial
40 cycles (Jost et al., 2005; Ludwig et al., 2018; Ramstein et al., 2007). Another long-term cycle of changes
41 due to high-frequency precession which drastically modified the hydrological patterns of this area
42 (monsoon, sapropels) is also superimposed.

43
44 Due to the peculiarities of both the atmospheric and oceanic circulation in the region, high-quality
45 climate modelling of the Mediterranean region needs to have high spatial resolution (Li et al., 2006).
46 Indeed, the presence of strong gusts of wind in winter are essential to trigger oceanic convection and
47 these can only be correctly represented in high-resolution models. Limited area models (LAM), or
48 regional climate models (RCM), present some advantages in this regard, since they generally demand
49 less computing resources, allowing them to be run at high spatial resolution for a given region. However,
50 their usefulness for paleoclimate purposes is limited because of the lack of adequate lateral boundary
51 conditions to drive the RCMs. The main reason why few comprehensive modelling exercises to explain
52 paleoclimate changes around the Mediterranean have been performed is that the level of computing
53 resources required for high resolution and long simulations is inaccessible. This is especially true in the
54 case of the Mediterranean Thermohaline Circulation (MTC), which has significantly changed in the
55 past, at both centennial and millennial scales.

56
57 Here we describe a modelling suite to define high-resolution atmospheric conditions over the
58 Mediterranean basin from global ESM (Earth System Model) paleoclimate simulations. This
59 atmospheric forcing can then be used to run a highly resolved ocean model (NEMOMED8 1/8°) to
60 accurately simulate ocean dynamics. This tool allows us to achieve a high spatial resolution and
61 equilibrated simulations with a run time of 100 years. The objective of this study is to develop a
62 modelling platform sufficiently comprehensive to conduct paleoclimate studies of the Mediterranean
63 basin. The potential of this platform is illustrated by investigating climate situations from the present
64 period and from the Early Holocene that is supposed to generate sapropel events.

65
66 The sapropel events provide excellent case studies on the impact of global changes on the Mediterranean
67 basin. These periodic events are related to a long period of anoxia of the deep and bottom waters
68 triggered by an enhancement of the African monsoon caused by periodicities of the orbital precession.
69 However, the localisation of the forcing source caused by orbital variability is still a subject of debate.
70 This is especially true for the last sapropel, denoted S1, which occurred during the early Holocene
71 (between 10500 and 6800 ka BP) (De Lange et al., 2008). Reproducing past climate variations over the

72 Mediterranean basin, including the sapropel events, is therefore a challenge for the modelling
73 community.

74

75 The paper is organised as follows: In the first section, we briefly review the different approaches used
76 to simulate the Mediterranean climate and sea conditions, and we also present the concept of the
77 sequential procedure that we propose. Section 2 presents in detail the model architecture we developed.
78 Finally, we present applications with simulations of the historical period (1970-1999) in Section 3 and
79 the Early Holocene (around 9.5 ka) in Section 4.

80 **1.2. Overview of current Mediterranean Sea modelling**

81 The Mediterranean Sea, due to its limited size and its semi-enclosed configuration, has a faster
82 equilibrium response (10^2 years) than the global ocean (10^3 years). Because of this semi-enclosed
83 configuration, there are a few requirements that modelling of the Mediterranean Sea needs to satisfy so
84 that its evolution can be properly represented. High resolution in both the atmospheric forcing and the
85 oceanic configuration is necessary to correctly simulate the convection areas and the associated
86 thermohaline circulation (Lebeaupin Brossier et al., 2011; Li et al., 2006). Depending on the mechanism
87 studied, the resolution of the ocean model used by the research community ranges from $1/4^\circ$ (e.g. for
88 paleo-climatic simulation), to $1/75^\circ$ (for hourly description of the mixed layer, tide-based investigation).
89 The results for oceanic convection are highly dependent on the flux of heat, flux of water, and the wind
90 stress at the air-sea interface especially the seasonal variability and intensity. There are many modelling
91 configurations in the scientific literature making it impossible to provide an exhaustive review of all of
92 them. We can summarise them by presenting the different approaches used to drive the Mediterranean
93 oceanic model, along with their advantages and drawbacks. We underline our new, coherent method,
94 which captures the changes in ocean dynamics in the Mediterranean basin derived from global
95 paleoclimate simulations.

96

97 *Observations and reanalysis*

98 The most common way to simulate the general circulation of the Mediterranean Sea is to run a regional
99 oceanic general circulation model forced by surface fluxes and wind stresses derived from observations
100 and reanalyses. In this way, an oceanic model can be driven by realistic fluxes. In most cases, this implies
101 an observation-based reconstruction of relevant variables with a spatial atmospheric resolution of less
102 than 50 km and a daily temporal resolution, at a minimum, in order to simulate the formation of dense
103 water (Artale, 2002). This approach is adapted to simulate the present-day Mediterranean Sea and to
104 explore the complexity of its sub-basin circulation and water mass formation (Millot and Taupier-
105 Letage, 2005). However, it is not well adapted to the study of past and future climate, partly due to the
106 excessive computing resources needed.

107

108 *Atmospheric model*

109 A second method consists of forcing a regional oceanic model with simulations from an atmospheric
110 model, AGCM (Atmospheric Global Climate Model) or ARCM (Atmospheric Regional Climate
111 Model). Since the AGCM resolution (typically 100 to 300 km horizontally) is coarse, statistical and/or
112 dynamical downscaling is usually needed, especially for wind-stress so that the ORCM (Ocean Regional
113 Circulation Model) can be correctly forced (Béranger et al., 2010). Currently, dynamical downscaling
114 with ARCM is the preferred option because it generally improves simulations of the climate in the
115 Mediterranean region and especially of the hydrological cycle (Li et al., 2012).

116

117 This configuration is broadly used to assess anthropogenic climate changes (Adloff et al., 2015; Macias
118 et al., 2015; Somot et al., 2006). In these studies, the Mediterranean Sea simulations are generally driven
119 by the outputs of an ARCM, which is, in turn, driven by the GCM or observation-based reanalysis. It
120 should be noted that biases in oceanic variables can be reduced through constant flux correction (Somot
121 et al., 2006). This configuration is suitable for high-resolution simulation of the past Mediterranean Sea
122 (Mikolajewicz, 2011 for the LGM; Adloff et al., 2011 for the Early Holocene among others).

123

124 *Regional coupled model*

125 Although the majority of the Mediterranean Sea models are ocean-alone models, some of them use a
126 coupled configuration between the Mediterranean Sea and the atmosphere. Such a coupled configuration
127 generally improves the simulation of the air-sea fluxes, including their annual cycle (de Zolt et al., 2003),
128 but may show climate drifts in key parameters such as the SST. Regional coupled models are now
129 emerging as a tool in Mediterranean climate modelling (Artale et al., 2010; Dell'Aquila et al., 2012;
130 Drobinski et al., 2012; Sevault et al., 2014; Somot et al., 2008). However, this full-coupling
131 configuration is currently not possible for high-resolution paleoclimate issues requiring long simulation
132 for hundreds or thousands of years.

133

134 *Importance of boundary conditions*

135 The boundary conditions applied to the Mediterranean Sea domain, in particular, the exchanges of water,
136 salt and heat with the Atlantic Ocean through the Strait of Gibraltar modulate significantly the
137 Mediterranean circulation (Adloff et al., 2015). This is especially true at the millennial scale where
138 deglaciation episodes and fluctuations of the AMOC (Atlantic Meridional Overturning Circulation) and
139 the Mediterranean Sea affect each other (Swingedouw et al., 2019). The level of discharge from the
140 main rivers is also crucial as is illustrated by the sapropel episodes, where an increase in freshwater
141 input drastically slowed down the MTC. Most of current models impose prescribed (observed when
142 possible) conditions in the near Atlantic zone, including temperature and salinity. The same
143 methodology can be used to prescribe river discharges. However, it must be acknowledged that

144 determining inputs from rivers into the Mediterranean Sea, either of water or other materials, still
145 presents serious challenges for modelling.

146 **1.3. Concepts for a sequential procedure to perform global-to-regional modelling**

147 In this paper, a new architecture for high-resolution modelling of the climate of the Mediterranean basin
148 for past, present and future conditions is proposed. This architecture is based on a method as much
149 consistency among the models as possible and high congruency with data.

150

151 *Step 1: Global climate*

152 Our goal is to simulate different climate conditions for the Mediterranean basin. The first step of any
153 relevant procedure should be to simulate the global climate conditions from which the simulation of the
154 regional climate is driven. These may be already available in simulations from previous PMIP exercises
155 for various periods (e.g. mid-Holocene, Last Glacial Maximum, Last Interglacial and mid-Pliocene) as
156 well as for different sapropel events and interglacials (e.g. MIS11, MIS13 and MIS19). However, this
157 is not always possible due to the large volume of high-frequency 3-D atmospheric circulation variables
158 involved. An alternative approach, used in some regional climate simulations (Chen et al., 2011;
159 Goubanova and Li, 2007; Krinner et al., 2014), consists of using an AGCM (either an independent one
160 or the same one used for the global climate simulation) run with appropriate values for global Sea
161 Surface Temperature (SST) and Sea Ice cover (SIC), derived from PMIP global simulations. SST is
162 crucial to determine atmospheric features and responses, while SIC plays a key role in determining the
163 global albedo. Monthly SST and SIC are necessary and sufficient to drive an AGCM. They can be
164 acquired from global climate simulations or through a bias-correction procedure.

165

166 *Step 2: Regional climate*

167 After running an AGCM, regional climate can be now reproduced with an ARCM nested into the high-
168 frequency outputs from the AGCM. Of course, the ARCM can be run in parallel to the AGCM, or with
169 a small time delay. Thus, we avoid a large accumulation of intermediate information between the AGCM
170 and the ARCM. In our study, we assume that there would be no feedback from the regional scale to the
171 global scale, so only a “one-way” transfer of information (from global to regional) is considered. In our
172 case, the ARCM is a strongly zoomed-in version of the AGCM and is also driven by monthly SST and
173 SIC values, as used for AGCM. The higher resolution of the ARCM allows the synoptic variability and
174 seasonality of the Mediterranean region to be depicted so that a realistic wind pattern and hydrological
175 cycle may be reproduced. This approach provides a general framework for use in many different
176 paleoclimate periods from the Pliocene to the Pleistocene, as long as the basin tectonics remain
177 unchanged.

178

179 *Step 3: Mediterranean Sea Circulation*

180 Daily air-sea fluxes and wind stress provided by the ARCM are used as surface boundary conditions to
181 drive the ORCM to investigate the oceanic dynamics of the Mediterranean. It is reasonable to assume
182 that the boundary conditions of these air-sea fluxes represent the long-term trends of the oceanic
183 dynamics. Rivers may be considered interactive or not depending on the investigative objectives: runoff
184 can be prescribed from climatology or obtained from the hydrological component of the surface model.
185 Again, we highlight that our architecture does not include any feedback, between either the regional
186 ocean and the regional atmosphere, or the regional ocean and the global ocean. This configuration means
187 that we can avoid dealing with certain issues, for example, the influence of the Mediterranean Outflow
188 Water on the North Atlantic Ocean but is well adapted to provide consistent river runoff associated with
189 changes in continental precipitation.

190 **2 Model architecture**

191 An ensemble of modelling tools that includes two atmospheric models and a regional oceanic model is
192 used. Figure 1 summarises the configuration and shows the experimental flowchart.

193 **2.1. The atmospheric models (AGCM and ARCM)**

194 LMDZ4 (Hourdin et al., 2006; Li, 1999) is the atmospheric general circulation model developed and
195 maintained by IPSL (Institut Pierre Simon Laplace). It has been widely used in previous phases of CMIP
196 and PMIP projects. The resolution of the model is variable. Its global version used here (referred to as
197 LMDZ4-global) is 3.75° in longitude and 2.5° in latitude with 19 layers in the vertical. It provides the
198 boundary conditions to drive LMDZ4-regional. LMDZ4-regional (Li et al., 2012) is a regionally-
199 oriented version of LMDZ4 with the same physics and same vertical discretisation, dedicated to the
200 Mediterranean region. The zoomed-in model covers an effective domain of 13°W to 43°E and 24°N to
201 56°N with a horizontal resolution of about 30 km inside the zoom. The rest of the globe outside this
202 domain is considered to be the buffer-zone for LMDZ4-regional where a relaxation operation is
203 performed to nudge the model with variables from the AGCM, at a 2-hour frequency. The resolution of
204 LMDZ4-regional decreases rapidly outside its effective domain. In both LMDZ4-global and LMDZ4-
205 regional, land-surface processes, including the hydrological cycle, are taken into account through a full
206 coupling with the surface model, ORCHIDEE (Krinner et al., 2005).

207 **2.2 The regional oceanic model (ORCM)**

208 NEMOMED8 (Beuvier et al., 2010; Herrmann et al., 2010) is the regional Mediterranean configuration
209 of the NEMO oceanic modelling platform (Madec, 2008). The horizontal domain includes the
210 Mediterranean Sea and the nearby Atlantic Ocean which serves as a buffer zone (from 11°W to 7.5°W).

211 The horizontal resolution is $1/8^\circ$ in longitude and $1/8^\circ \cos\phi$ in latitude, i.e. 9km to 12km from the north
212 to the south. The model has 43 layers of inhomogeneous thickness (from 7 m at the surface to 200 m in
213 the depths) in the vertical. River discharges are accounted for as freshwater fluxes in the grids
214 corresponding to the river mouths. A dataset of climatological river discharges is proposed by default
215 to cover the entire Mediterranean draining basin with 33 river mouths. It is of course switched off when
216 rivers are interactive in the platform. The interactive calculation of freshwater discharges from rivers by
217 the land-surface model, ORCHIDEE, includes 192 river mouths to cover the Mediterranean draining
218 basin. The Black Sea, not included in NEMOMED8, counts as a river dumping freshwater into the
219 Aegean. The deposit rate is calculated based on total runoff into the Black Sea, plus the net budget of
220 precipitation (P) minus evaporation (E) over the Black Sea.

221
222 When the oceanic model NEMO is used alone, with prescribed surface fluxes, it is indispensable to
223 implement a restoring term with a constant coefficient of $40 \text{ W.m}^{-2}.\text{K}^{-1}$. This is a standard procedure for
224 NEMO to prevent eventual run-away cases. In our modelling chain, the target temperature for the
225 restoration is the surface air temperature from the regional atmospheric model LMDZ4-regional.

226 **2.3 Modelling Sequence**

227 As shown in Fig. 1, the first step in our modelling chain is to obtain SST and SIC values from an Earth
228 System Model simulation able to reproduce global climate (for the past, present or future). We can
229 reasonably hypothesise that major global climate information can transit from global SST and SIC. This
230 hypothesis was deemed legitimate for climate downscaling purposes for Antarctic and Africa, in Krinner
231 et al. (2014) and Hernández-Díaz et al. (2017) respectively. In the present work we use IPSL-CM5A
232 (Dufresne et al., 2013) to extract relevant SST and SIC values to drive the AGCM (LMDZ4-global) and
233 the ARCM (LMDZ4-regional). The next step is to run the two atmospheric models, LMDZ4-global and
234 LMDZ4-regional, in the usual way as proposed by the AMIP community. This is the most expensive
235 step, as atmospheric models are the most demanding in terms of computing resources. Fortunately, it is
236 not necessary to run them for a long time as the atmosphere reaches equilibrium quickly. We applied 30
237 years of simulation to both models. We consider this duration to be long enough to depict climate
238 variability for the simulation of past events. The AGCM nudges the ARCM in the conventional way of
239 one-way nesting for temperature, humidity, meridional and zonal wind every two hours. The nudging is
240 done using an exponential relaxation procedure with a timescale of half an hour outside the zoom and
241 10 days inside the zoom. Table S2 in the SOM summarises the forcings used, especially the orbital
242 forcing and atmospheric CO_2 .

243 The necessary variables (surface air temperature, wind stress, P-E over the sea, heat fluxes) are provided
244 by ARCM to NEMOMED8 (ORCM) at daily frequency. The salinity and temperature conditions are
245 provided in three dimensions in the Atlantic buffer zone, near the Gibraltar Strait, and updated every

246 month. River runoff, updated every month, depends on the configuration used (prescribed climatological
247 rivers, or interactive rivers). Table S3 in SOM details these boundary conditions.

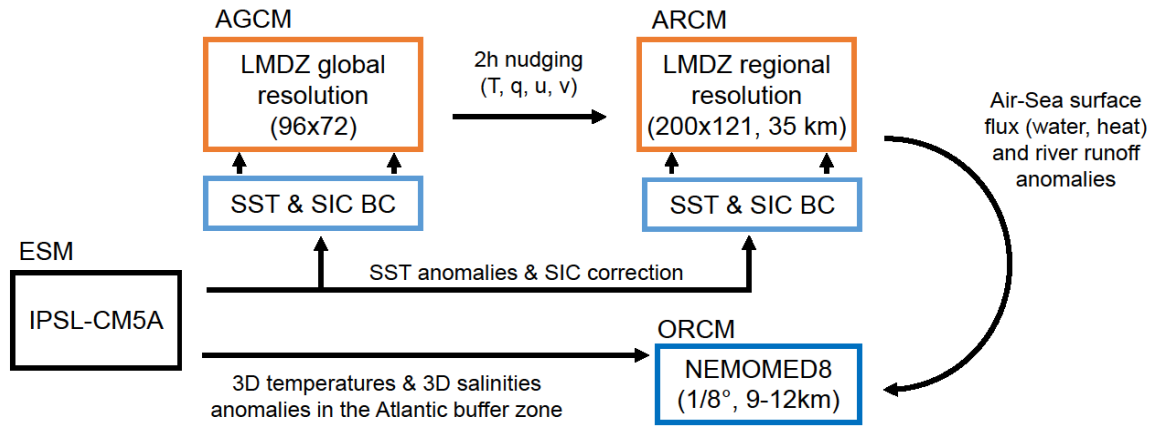
248 It is worthy to mention the work of Mikolajewicz (2011) who used a similar modelling chain (from a
249 coarse-resolution earth system model to a high-resolution regional oceanic model) to simulate the
250 Mediterranean Sea climate during the last glacial maximum. However, Mikolajewicz (2011) used only
251 an AGCM (ECHAM5) as the intermediate step. In our case, we found that the use of ARCM was
252 indispensable to produce high-quality forcing to correctly simulate the oceanic convection in
253 NEMOMED8.

254 **2.4 Bias correction**

255 The sequential modelling chain, despite the lack of interactivity and feedback at interfaces, allows for
256 error removal and bias correction at each step of the methodology. This adjustment is sometimes crucial,
257 especially when model outputs need to be of very high quality to be incorporated into impact studies.
258 This concept was further described in Krinner et al. (2019), as illustrated in Fig. 16 of their paper.
259 Therefore, to enhance our confidence in the realism of the simulation results, bias-correction may be
260 introduced when necessary. The correction method used in the present work generally follows the
261 conventional procedure, which is based on the difference between the model outputs for present day
262 simulations and actual observations. Biases corrected in this way, theoretically only valid for the
263 historical simulation (named HIST hereafter), are assumed to remain unchanged for past and future
264 simulation scenarios. However, the transferability between past and future periods is questionable. There
265 is no guarantee that the model error for one period is the same for other periods, even though the model
266 physics may be the same. In addition, paleodata are often rare and incomplete, and so, are unsuitable for
267 evaluation and correction of model errors. The most reliable basis is that established for the present day.
268 The reader can find a full description of the bias corrections and their eventual use in our applications
269 in the supplementary online material, “Text S2: Bias correction”.

270

271



272

273

274 **Figure 1: Flowchart of the modelling chain including the four main components generally**
 275 **represented by ESM, AGCM, ARCM and ORCM, respectively, and actually implemented in our**
 276 **platform by IPSL-CM5A, LMDZ-global, LMDZ-regional and NEMOMED8. BC: boundary**
 277 **condition, u: zonal wind, v: meridional wind, q: specific humidity, T: temperature, S: salinity,**
 278 **SST: sea surface temperature, SIC: sea-ice concentration.**

279 **3 Validation of the modelling chain for present-day climate 1970-1999**

280 In this section, the capacity of the model to reproduce the climate of the recent past is evaluated, in
 281 particular, its ability to simulate sea surface characteristics as well as the Mixed Layer Depth (MLD)
 282 and oceanic convection patterns as these are key elements to reproduce the evolution of the
 283 Mediterranean Sea in past climate conditions.

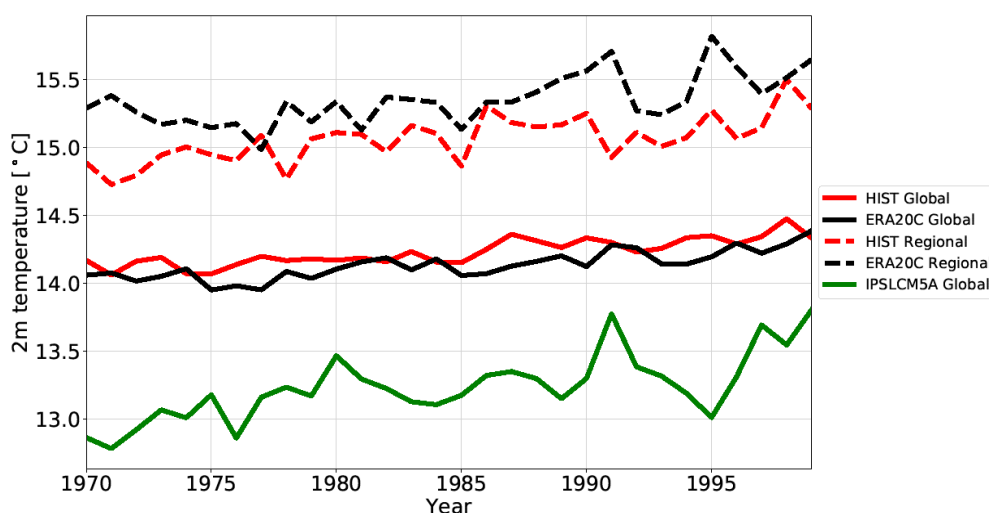
284 **3.1 Experimental design**

285 For the HIST experiment, SST and SIC observations (ERA-Interim, Dee et al., 2011) are used to force
 286 the AGCM. River runoff is from the climatology of Ludwig et al., (2009). Monthly mean climatological
 287 sea temperatures and salinities (World Ocean Atlas database from Locarnini et al., 2013, Zweng et al.,
 288 2013) are used for the Atlantic boundary zone. HIST atmospheric simulations for both global and
 289 regional simulations have a duration of 30 years. The length of the HIST oceanic simulation is also 30
 290 years, but obtained after a 150-year spin-up. The forcings for each experiment are detailed in “Tables
 291 S2 and S3” in the supplementary online material. Spin-up phases for each simulation are also shown
 292 from “Figure S4” to “Figure S8” for the overturning stream function and the index of stratification.

293 **3.2 Evolution of temperatures**

294 Figure 2 depicts the temporal evolution, between 1970 and 1999, of annual mean surface air
295 temperatures at two metres in the atmospheric simulations (global and regional) compared to
296 observations for the whole globe and over the Mediterranean region. The two models reproduce a range
297 of temperatures similar to the observations, with the Mediterranean temperatures warmer than the global
298 temperatures. The global simulation, after SST bias correction, ranged with the observation, compared
299 to IPSLCM5A (Figure 2). The regional model reproduces the warming trend and aspects of the
300 interannual variability which are quite close to observations.

301
302

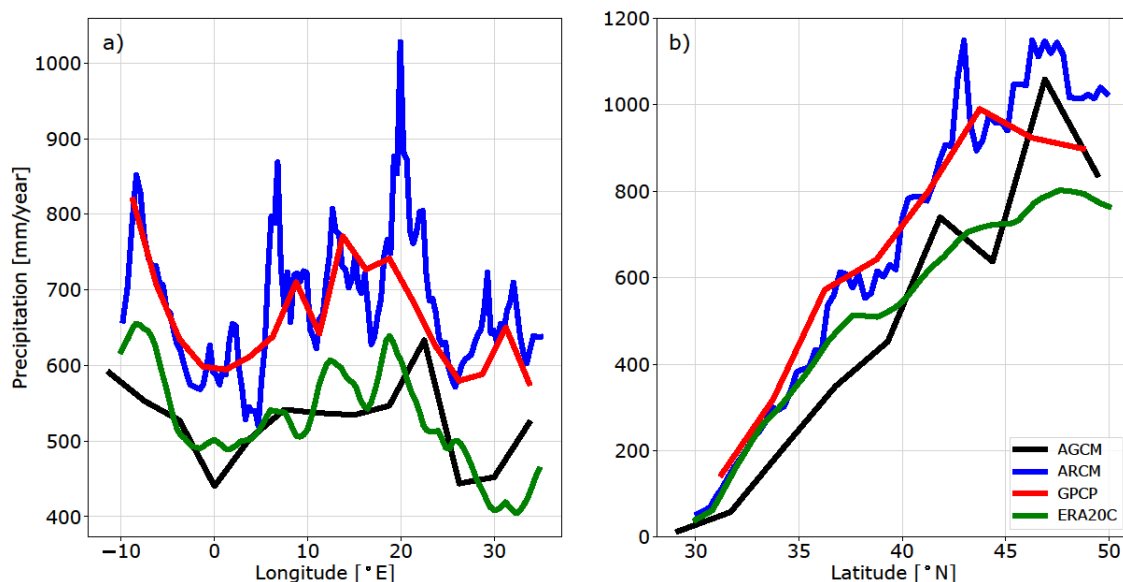


303
304 **Figure 2: Time series of annual mean surface air temperatures at 2 m in HIST (red) and ERA20C**
305 **(black, ref: Stickler et al., 2014) and IPSLCM5A (green) for global average (solid lines) and**
306 **Mediterranean-region (ocean and continent) average (dashed lines).**

307 **3.3 Precipitation and freshwater budget**

308 Figure 3 a and b show the average annual precipitation for 1970-1999 in HIST over the Mediterranean
309 region and the differences with observations. The main features of the distribution of precipitation over
310 the Mediterranean region are simulated, in particular the distinct contrast between the very low
311 precipitation in the southern region and higher precipitation in the north. The ARCM tends to generate
312 higher precipitation than the AGCM due to the resolution refinement. Compared to observation, AGCM
313 is closer to ERA20C (Stickler et al., 2014), whereas ARCM is closer to GPCP data (Adler et al., 2018).
314 However, the regional model still overestimates the amount of precipitation, especially at 42°N, from
315 45° to 50° N, at 8°E and 20°E. It corresponds to most of Europe, especially over the Alps, the Pyrenees,
316 the Balkans and other mountainous regions. The freshwater budget over the Mediterranean Sea from

317 observations (a synthesis from Sanchez-Gomez et al., 2011 and from other sources) and in the various
 318 simulations conducted in this study are summed up in Table 1. The simulated continental precipitation
 319 is overestimated, but both the precipitation and evaporation over the Mediterranean Sea in HIST is very
 320 close to the observations. Two other simulations, PICTRL and EHOL, are those designed in Section 4
 321 to investigate the Early Holocene climate.
 322



323
 324
 325 **Figure 3: Annual mean precipitation, a) meridionally averaged (30 to 50°N), b) zonally averaged**
 326 **(-10 to 35°E), in the historical simulations with AGCM (LMDZ-global) and ARCM (LMDZ-**
 327 **regional). Observation comes from GPCP (Global Precipitation Climatology Project, 1979 to**
 328 **1999, blue line, ref: Adler et al., 2018). and ERA20C (green line, ref: Stickler et al., 2014).**
 329

Dataset or experiment	E	P	R	B	E - P - R - B
OBS	1096-1136	256-595	102-142	73-121	238-705
HIST	1106	443	74	104	485
PICTRL	1031	451	98	104	378
EHOL	1094	460	225	104	305

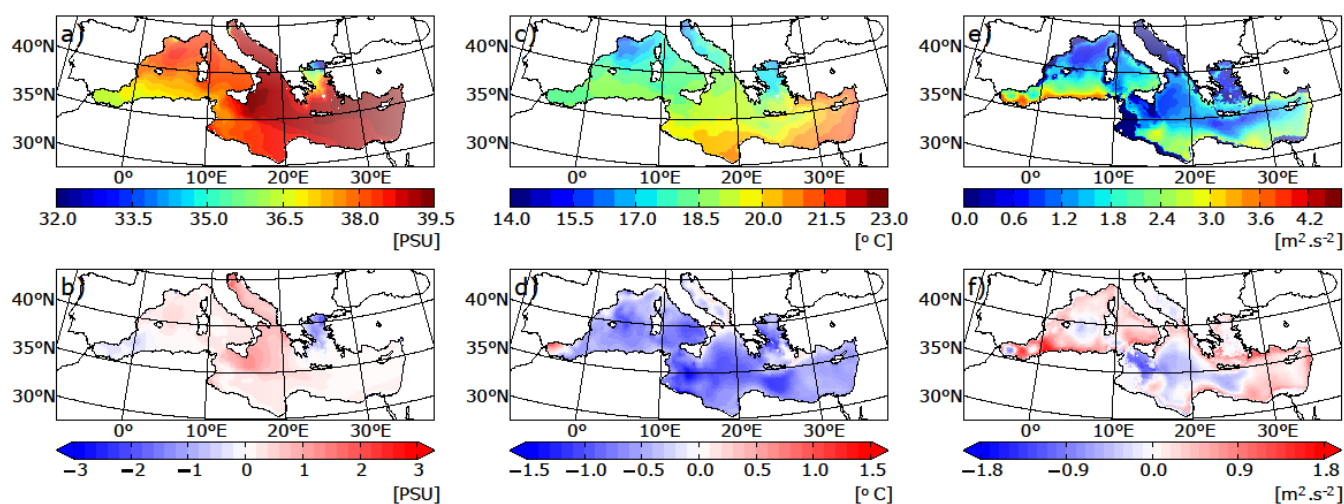
330 **Table 1: The Mediterranean Sea freshwater budget, expressed as mm.year⁻¹ for the whole water**
 331 **area (about 2.5 million of km²). E, evaporation, P, precipitation, R, river runoff, B, Black Sea**
 332 **discharge into the Mediterranean Sea. OBS is a summary from Sanchez-Gomez et al., (2011) for**
 333 **P, E and P-E, from Ludwig et al., (2009) for R, from Lacombe and Tchernia, (1972), Stanev et al.,**

334 (2000) and Kourafalou and Barbopoulos, (2003) for B. River discharges in HIST are from the
 335 climatology of Ludwig et al., (2009). PICTRL uses the Nile of its pre-industrial (pre-damming)
 336 value, $2930 \text{ m}^3 \cdot \text{s}^{-1}$, annually (Rivdis database, Vorosmarty et al., 1998). River discharges in EHOL
 337 are deduced from the difference between EHOL and PICTRL.
 338

339 3.4 Mediterranean Sea surface characteristics

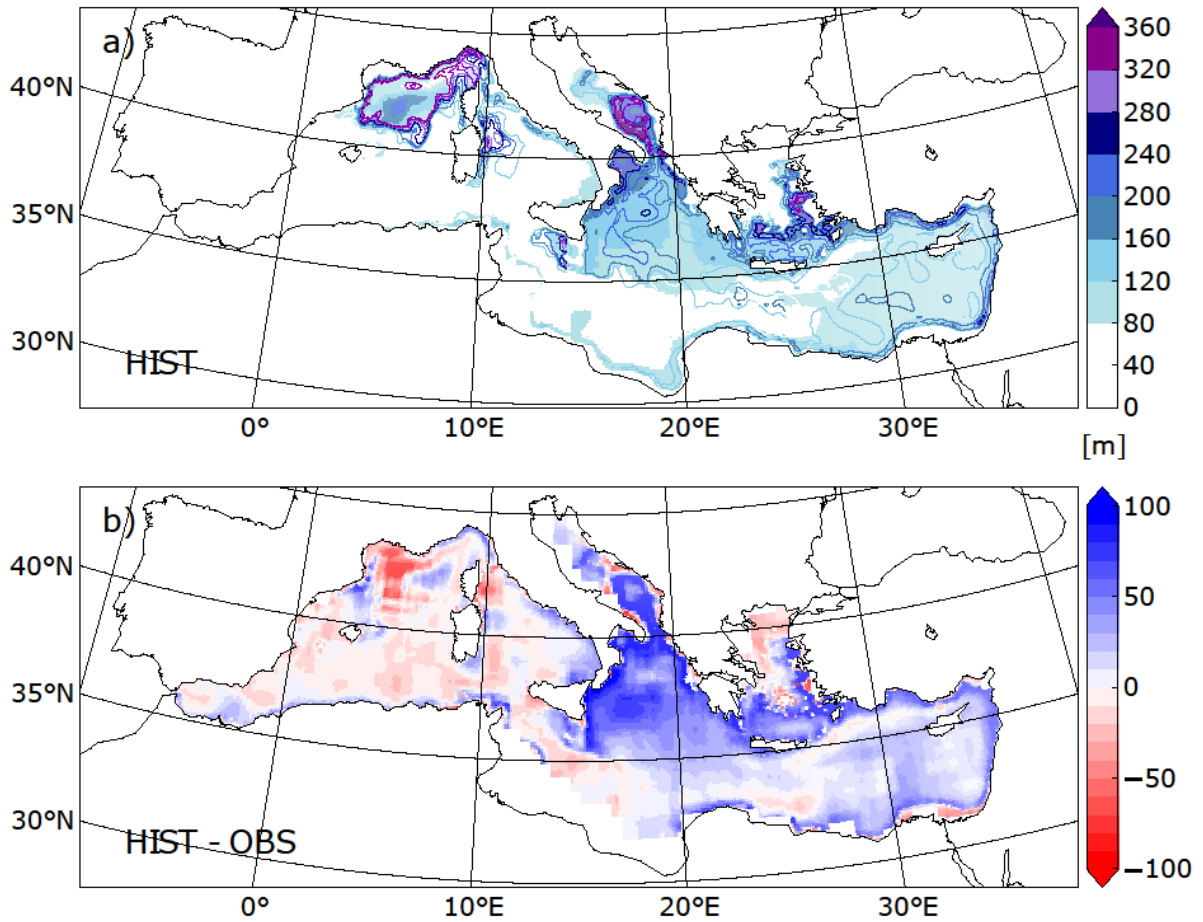
340 Figure 4 displays the temperatures and salinities of the Mediterranean Sea simulated in HIST and the
 341 deviations from observations. The model is able to capture the main characteristics of the pronounced
 342 west-east gradient of SSS in the Mediterranean Sea (Figure 4 a). Values are within the range of
 343 observations (mean bias = 0.32 PSU, error = 0.37 PSU, table 2). In the simulation, the Aegean Sea is
 344 not salty enough (about -1.5 PSU) and the Adriatic/Ionian Sea is too salty (+1 PSU).
 345 The model reproduced the northwest to southeast temperature gradient, as shown in Figure 4b. However,
 346 the model shows a general cold bias (from -0.5 to -1.5 °C) over the entire Mediterranean (Figure 4e),
 347 due to the cold bias already observed for the air temperature at 2m in the regional atmospheric forcing
 348 (cf Figure 2).

349
 350



351
 352 **Figure 4: Annual mean sea-surface salinity (left panels, SSS in PSU), sea-surface temperature**
 353 **(middle panels, SST in °C) and index of water column stratification (right panels, winter IS in**
 354 **$\text{m}^2 \cdot \text{s}^{-2}$) simulated in HIST (top panels) and the HIST deviation (model – obs) from the observation-**
 355 **based MEDATLAS data (averaged over the entire simulation).**

356
 357



358
 359 **Figure 5: a) Mixed layer depth simulated in HIST (panel a, in m) and as deviation (b) of HIST**
 360 **from observations of Houpert et al., (2015) averaged over the entire simulation for JFM (January**
 361 **February March). Contour lines in the upper panel a) represents the maximum of MLD**
 362 **throughout the HIST simulation.**

363

	SST (°C)	SSS (PSU)	IS (m ² .s ⁻²)
Mean bias (model – obs)	-0.64	0.32	0.91
RMS error	0.45	0.37	0.29

364

365 **Table 2: Mean biases of sea surface temperature (SST), sea surface salinity (SSS) and index of**
 366 **stratification (IS) in the HIST simulation, expressed as the deviation from observations**
 367 **(MEDATLAS-II), and associated root mean square errors.**

368 3.4 Mediterranean Thermohaline circulation

369 Here, the general characteristics of the simulated thermohaline circulation is evaluated in regions where
370 deep and intermediate water formation occurs. Figure 4c displays the stratification index (IS¹) for HIST.
371 IS is a vertical integration of the Brunt-Vaisala frequency. A lower IS implies that convection is more
372 likely. The range of IS biases (Figure 4f), is from -1 to 1 m².s⁻² (mean bias = 0.91 m².s⁻², error = 0.29
373 m².s⁻²). The model satisfactorily reproduces the convection in known intermediate and deep-water
374 formation areas, namely the Gulf of Lions, the Adriatic Sea, the Ionian Sea, the Aegean Sea and the
375 North Levantine.

376

377 Comparison with observations of the mixed-layer depth (Houpert et al., 2015) confirms that the model
378 reproduces realistic intermediate and deep-water formation patterns, with a thicker MLD in the eastern
379 basin, due to salty condition (Figure 4a and e), and a shallower MLD in the Gulf of Lions (figure 5b).

380

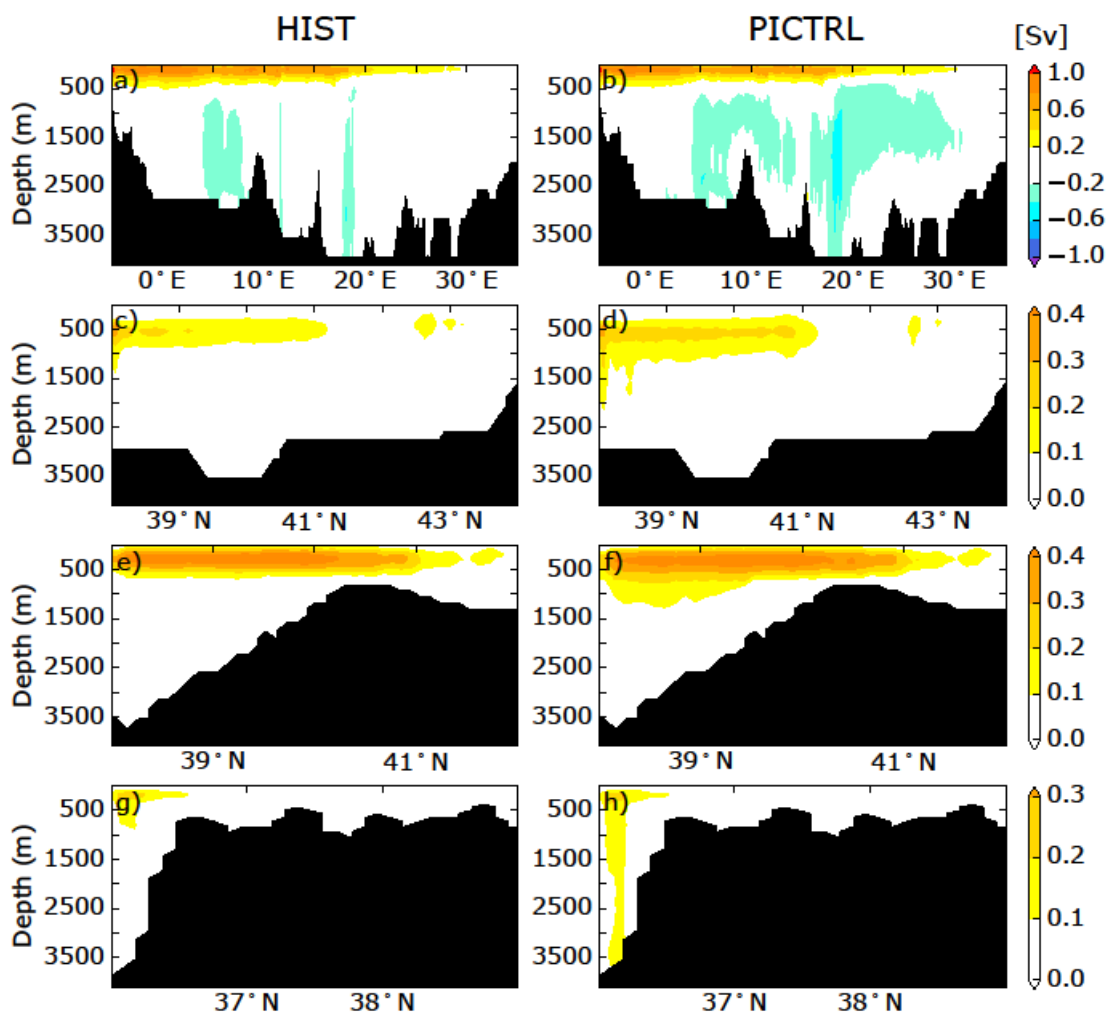
381 The simulated Mediterranean overturning circulation is analysed (figure 6). The Zonal Overturning
382 stream Function (ZOF²) in figure 6a depicts the surface and intermediate circulation and the
383 intermediate/deep circulation. The surface current from the Strait of Gibraltar flows up to 30°E and back
384 to the Atlantic Ocean in the intermediate layers, through the Levantine Intermediate Water (LIW)
385 outflow. Figure 6 c, e, and g represents the Meridional Overturning stream Function (MOF³) in the Gulf
386 of Lions, the Adriatic Sea and the Aegean Sea, respectively. The surface cell in the longitude-depth plan
387 is comparable to previous studies done with the same regional oceanic model, but with different forcings
388 (Adloff et al., 2015; Somot et al., 2006): the mean strength of the surface cell ranges from 0.8 to 1.0 Sv,
389 and the longitudinal extension is from 5°W to 30°E. The simulated intermediate and deep cells are
390 recognized in existing studies as having different characteristics. Our simulated pattern is very close to
391 a similar historical run in Adloff et al., (2015), but is weaker than a historical run in Somot et al., (2006),
392 and a second historical configuration (with refined air-sea flux) in Adloff et al., (2015). The ZOF

¹ $IS(x, y, h) = \int_0^h N^2(x, y) z dz$. N^2 is the Brunt-Väisälä frequency. IS is calculated at each model grid (x, y) for a given depth h (set as the bottom of the sea, or as 1000 m when the depth is greater than 1000 m).

² $ZOF(x, z) = \int_h^z \int_{y_s}^{y_n} u(x, y, z) dy dz$. u is the zonal currents, h is the depth of the bottom, y_n and y_s are the north and south coordinates respectively.

³ $MOF(y, z) = \int_h^z \int_{x_e}^{x_w} v(x, y, z) dx dz$. v is the meridional currents, h is the depth of the bottom, x_w and x_e are the west and east coordinates respectively.

393 depicted in HIST is consistent with the reanalyses (1987-2013) of Pinardi et al. (2019) over the Western
 394 basin, but shows a weaker Eastern deep cell compared to the reconstruction.
 395



396
 397 **Figure 6: Zonal Overturning stream-Function (ZOF, first row , panels a, and b) integrated from**
 398 **north to south and shown as a longitude-depth section for the whole Mediterranean Sea, for HIST,**
 399 **and PICTRL simulations (from top to bottom), respectively. Other panels show Meridional**
 400 **Overturning stream-Function (MOF) shown as a latitude-depth section, integrated west/east for**
 401 **the Gulf of Lion (second row, longitudinal extent: 4.5° to 8°E), the Adriatic/Ionian Sea (third row,**
 402 **12° to 21°E), and the Aegean Sea (fourth row, 24° to 28°E) averaged over the entire simulation for**
 403 **HIST and over the last 30 years of simulation for PICTRL.**

404 **3.5 Summary of Validation**

405 Validation of our platform was based on the historical period, 1970 to 1999. The atmospheric simulation
406 is acceptable compared with observations for the air temperature at 2m at both global and regional scales.
407 The simulated precipitation from the atmospheric models produces a signal that ranges with the
408 observation, but there is significant overestimation of precipitation over the mountainous area and over
409 the land surrounding the Mediterranean Sea. However, the freshwater budget over the sea is close to
410 observations for both evaporation and precipitation. The areas of intermediate and deep convection
411 produced by the model are realistic, and the simulation of the thermohaline circulation is well captured
412 by the oceanic model and in the range of the state-of-the-art existing Mediterranean regional models
413 (compared to the simulations of Adloff et al., 2015 and Somot et al., 2006 for instance) and reanalysis
414 as well (Pinaridi et al., 2019). These features inspire confidence in our modelling platform for the
415 investigations of past climate.

416 **4 Application of the modelling chain to the Early Holocene**

417 In this section, results obtained when our sequential modelling chain is applied in a paleoclimate context
418 are presented, which was our initial motivation for developing this modelling tool. We chose to test the
419 performance of our tool on the Early Holocene, a period marked by significant changes in climate and
420 ocean dynamics over the Mediterranean basin, when the last sapropel event, S1, occurred in the
421 Mediterranean Sea. Our experimental design relies on the comparison of two simulations: the Early
422 Holocene (EHOL) with PICTRL based on pre-industrial conditions, the latter acting as a reference.

423 **4.1 Experimental design**

424 As indicated in the general flowchart of our modelling platform, global SST and SIC are required to
425 initiate our sequential modelling. The basic assumption is that the climate change signal can be
426 reconstructed from global SST and SIC, an accepted practice within the climate modelling community.
427 In this study, two existing long-term coupled simulations from IPSL-CM5A is used, one covering the
428 pre-industrial period and the other covering the Early Holocene (around 9.5 ka). Taking the last 100
429 years of each simulation, a climatological SST and SIC is constructed. After conducting bias-correction,
430 these outputs from IPSL-CM5A are then used to drive the AGCM (LMDZ-global) and the ARCM
431 (LMDZ-regional) in a further step. The duration of the PICTRL and EHOL atmospheric simulations is
432 30 years (both global and regional models).

433
434 Oceanic temperature and salinity in the Atlantic buffer-zone, as well as freshwater discharges from
435 Mediterranean rivers, are all bias-corrected for NEMOMED8, as described in the general methodology.
436 However, it needs to be pointed out that the reference point for the Nile river discharge is not modern

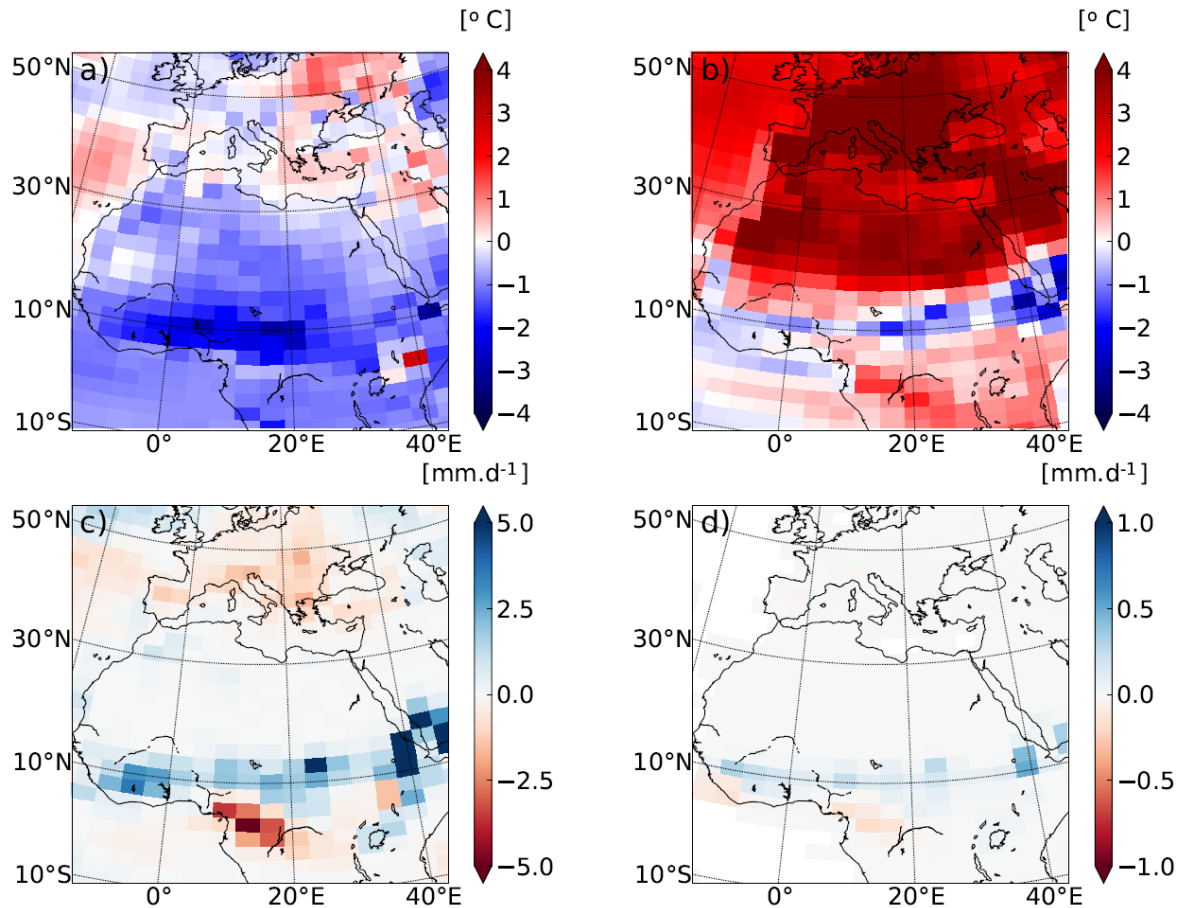
437 observations but is set at pre-industrial values ($2930 \text{ m}^3 \cdot \text{s}^{-1}$ for annual mean, Vorosmarty et al., 1998)
438 corresponding to a period before construction of the Aswan dam. The oceanic simulation is 90 years for
439 EHOL and 30 years for PICTRL, performed after a 200-year spin-up of PICTRL.

440 **4.2 Climate features depicted in LMDZ-global (AGCM)**

441 Because Early Holocene simulations are mainly driven by insolation forcing, an important feature is the
442 model response to seasonal temperatures. Figure 7 shows the difference between EHOL and PICTRL,
443 as reproduced in the AGCM, LMDZ-global, for the summer/winter temperature, JJAS precipitation and
444 JAS surface runoff. The atmospheric model imprints a stronger seasonality due to the increased Early
445 Holocene summer insolation. Warmer summer temperatures over Europe and North Africa ($+ 6 \text{ }^\circ\text{C}$,
446 figure 7b) and lower winter temperatures over Africa ($-2 \text{ }^\circ\text{C}$, figure 7a) reflect this feature. Variations
447 of the precession also trigger an enhancement of the African Monsoon ($+ 10 \text{ mm} \cdot \text{day}^{-1}$ over the Ethiopian
448 region, figure 7c). The main consequence of this increase in precipitation is an enhanced surface runoff
449 over the Ethiopian region. This hydrological state is similar to the African Humid Period caused by the
450 enhanced African Monsoon and the resultant increase in surface runoff, as shown in Rossignol-Strick et
451 al. (1982).

452

453 Our results are similar to those of previous modelling exercises for the Early- and Mid-Holocene (e.g.
454 Adloff et al., 2011; Bosmans et al., 2012; Braconnot et al., 2007; Marzin and Braconnot, 2009). They
455 are also consistent with various reconstructions of mid-Holocene precipitation (Harrison et al., 2014).
456 A detailed comparison can be made with the Early Holocene simulation reported in Marzin and
457 Braconnot (2009) which used for their experiment the same orbital parameters and the same atmospheric
458 model as EHOL. However, their model was coupled to an oceanic model, while an atmospheric model
459 and prescribed SST and SIC as boundary conditions are used in this study. Generally speaking, our
460 results for both surface air temperature and precipitation are very similar to those of Marzin and
461 Braconnot (2009), attesting to the validity of our approach using a simple atmospheric model
462 constrained by boundary conditions. In the ensemble of PMIP simulations, available for the Early
463 Holocene and mid-Holocene, there are some robust outputs for the climate response to orbital forcing
464 but there are also some weaknesses common to most of the models (Braconnot et al., 2007; Kageyama
465 et al., 2013). One of these weaknesses is the underestimation of the spread of the African monsoon
466 towards North Africa. However, the increased discharge from the Nile river, induced by the enhanced
467 monsoon is well supported by data (Adamson et al., 1980; Revel et al., 2014; Williams, 2000).



468

469

470 **Figure 7: Temperature and precipitation deviations of EHOL from PICTRL in LMDZ-global, the**
 471 **AGCM for a) winter surface air temperatures at 2 m, b) summer surface air temperatures at 2 m,**
 472 **c) June to August precipitation, and d) July to September surface runoff (averaged over the entire**
 473 **simulation).**

474 4.3 Mediterranean climate features with dynamical downscaling refinement

475 Figures 8, 9 and 10 show the results from the regional atmospheric model (LMDZ-regional), compared
 476 to those from LMDZ-global for PICTRL and EHOL over the Mediterranean region. In both the global
 477 and regional simulations, an increased seasonality is depicted, with warmer summer (+2 to +6 °C) and
 478 colder winter, especially over land (-3 to -1 °C, Figure 8). Downscaling with LMDZ-regional slightly
 479 reduces the amplitude of the summer warming and shows a more homogenous signal in winter over
 480 land. The general circulation of the surface wind in PICTRL is west to east (Figure 9b), in line with the
 481 dominant winter regime of westerlies in the region. This important feature is almost missed in the global
 482 model (Figure 9a) which reproduces a lower intensity than the regional model. The winter precipitation
 483 in EHOL, for ARCM (LMDZ-regional), increases over land in the Balkans and Italy and over the
 484 Adriatic, Ionian and Aegean Seas (Figure 10b). These changes are also present in the AGCM (LMDZ-

485 global) that, furthermore, shows an increase in Spain and Portugal (Figure 10a). It is in summer that the
486 two models show the largest differences. In ARCM (LMDZ-regional), the Mediterranean basin
487 experiences drier conditions, except in Italy and the North of the Balkans. Over the sea, precipitations
488 slightly increase in EHOL (Figure 10). However, the AGCM (LMDZ-global) shows drier conditions in
489 the northern two thirds of the Mediterranean domain, with more humid conditions in the southern third
490 (Figure 10c). Changes in precipitation lead to unavoidable modifications in the runoff and river
491 discharge into the Mediterranean Sea.

492

493 Although it is not straightforward to compare our “snapshot” simulations against environmental records
494 (often used to reconstruct a timeline), our results compare well with the available data for this area (see
495 supplementary online material, “Text S3: Comparison of model simulation outputs and reconstructed
496 data for the Mediterranean basin”). Numerous proxies provide information on lake levels, paleo fires,
497 pollen, isotopic signals recovered from speleothems which together describe the Mediterranean climate
498 in the past. All of these proxies need to be brought together to provide a clear impression of the
499 Mediterranean climate for this period (Magny et al., 2013; Peyron et al., 2011). Magny et al. (2007),
500 based on records from Lake Acessa (Italy), suggested that aridification took place around 9200–7700
501 cal BP. Zanchetta et al. (2007), based on data recovered from speleothems in Italy, conclude that the
502 Western Mediterranean basin experienced enhanced rainfall during the S1 (10000-7000 cal BP). Jalut
503 et al. (2009), using pollen data, suggest that the summers were short and dry and that there was abundant
504 rainfall in winter (autumn and spring as well) and remarked that these wetter conditions favoured broad-
505 leaf tree vegetation. Different proxies seem to provide contradictory information and therefore,
506 seasonality must be introduced to reconcile them. Peyron et al., (2011) mentioned wet winters and dry
507 summers during the ‘Holocene optimum’. Magny et al., (2013) support the hypothesis of seasonal
508 contrast based on the analysis of multi-proxies.

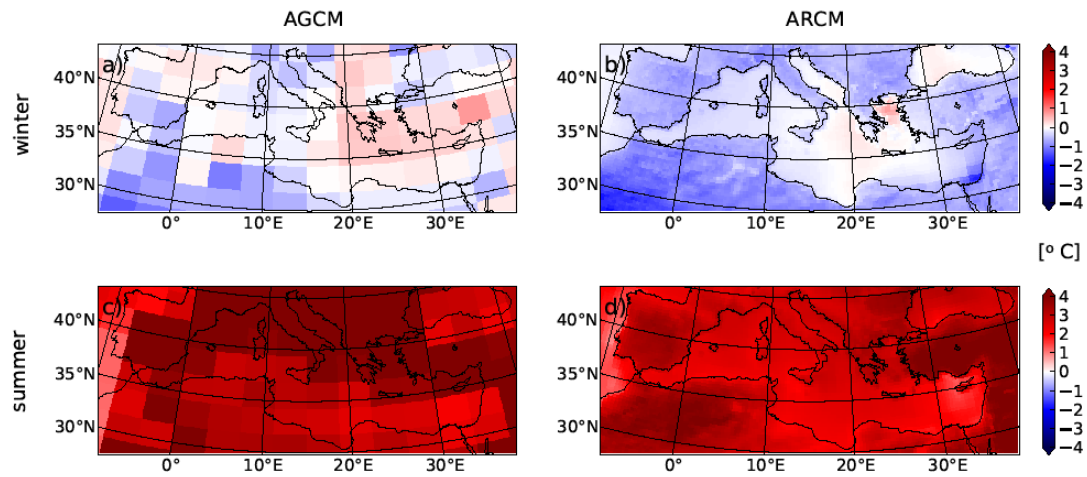
509

510 Our EHOL simulation successfully depicts this temperature contrast between winter and summer.
511 Precipitation is enhanced in winter. In summer, the Mediterranean region is globally drier, except over
512 Northern Italy and the northern Balkans. As explained above, there is no precipitation signal over
513 Northern Africa, although evidence of paleo-lakes has been found in Algeria (Callot and Fontugne,
514 1992; Petit-Maire et al., 1991), Tunisia (Fontes and Gasse, 1991) and Libya (Gaven et al., 1981; Lézine
515 and Casanova, 1991) during the Early Holocene indicating increased rainfall in this area. In the
516 supplementary material, a comparison between simulated continental precipitation outputs and pollen
517 reconstruction data is provided. This comparison shows that the winter precipitation anomalies are
518 consistent in both cases but that there is a distinct difference in summer values due to the more contrasted
519 summer in the EHOL simulation.

520

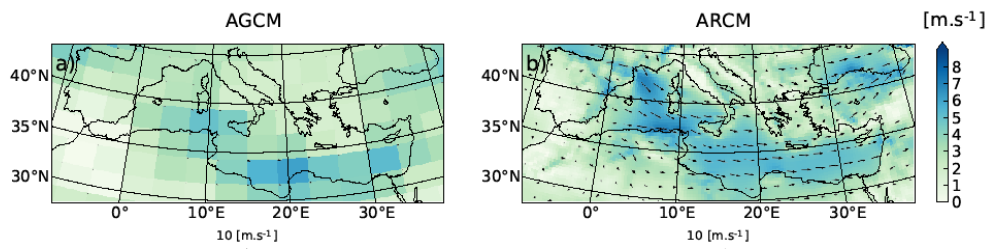
521

522
523



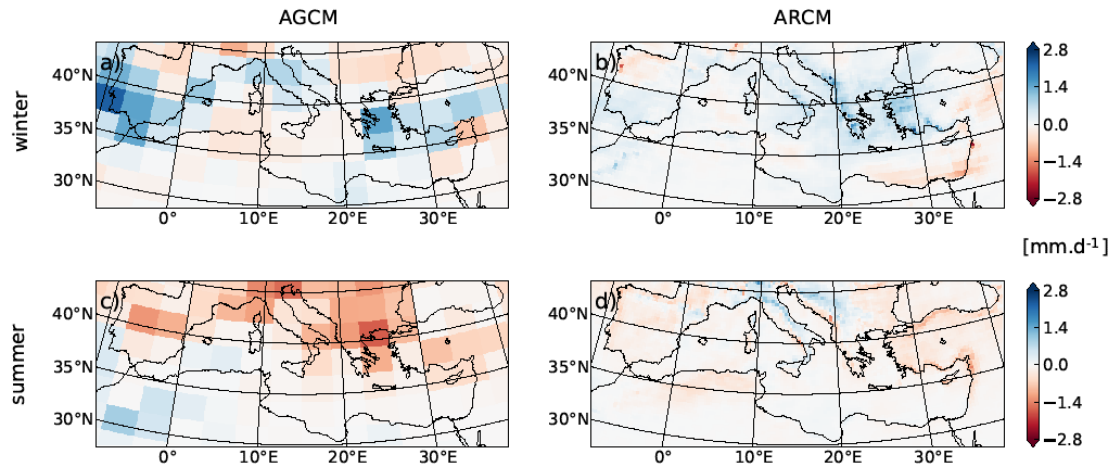
524
525
526
527
528
529

Figure 8: Deviations (EHOL – PICTRL, averaged over the entire simulation) of surface air temperature at 2 m for winter (upper panels) and summer (lower panels), respectively. AGCM (LMDZ-global) is displayed on the left and ARCM (LMDZ-regional) on the right.



530
531
532

Figure 9: Winter wind-speed in PICTRL for a) the AGCM and b) the ARCM.



533

534 **Figure 10: Same as in Figure 8, but for precipitation rate (mm/day).**

535 **4.4 Hydrological changes**

536

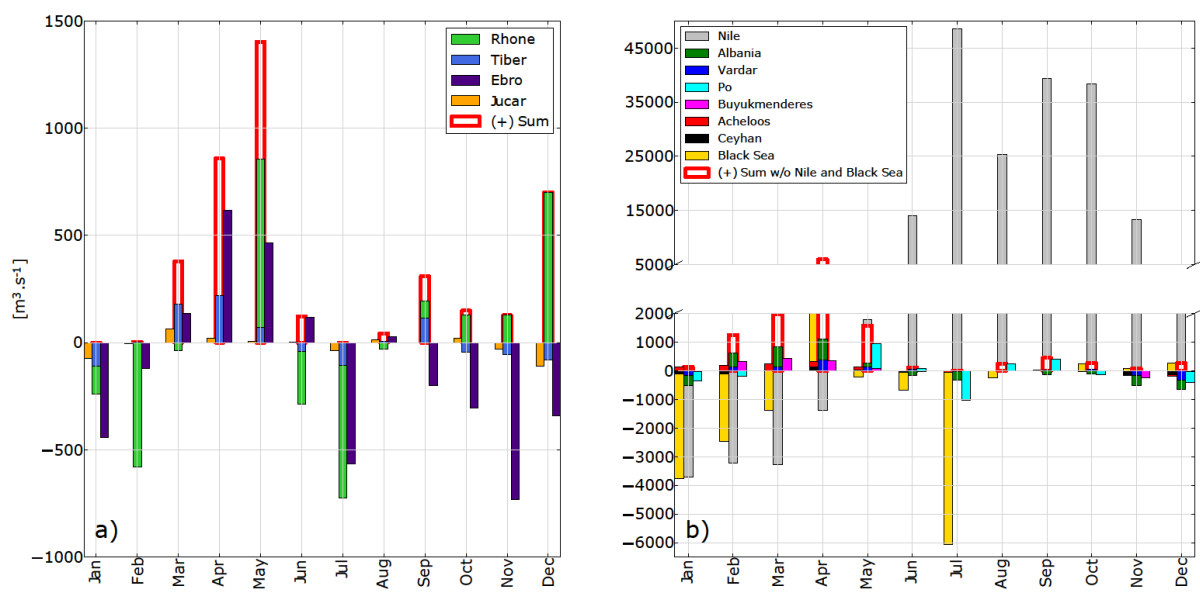
537

538 Figure 11 shows anomalies (EHOL – PICTRL) of river freshwater supplies into the Mediterranean basin
 539 as simulated by the ARCM (LMDZ-regional). Bars are displayed for each calendar month to show the
 540 strong seasonal variation, and for the western and eastern basins separately. Due to their particular role
 541 and their specific treatment in our current modelling practice, the Nile and the Black Sea are also shown
 542 for the eastern basin, but not accounted in the sum. The North African rivers are not displayed since
 543 they don't show much changes for their catchment area. The Nile River shows important seasonal
 544 variation, with increase in summer and autumn and decrease in winter and spring. The Albanian rivers
 545 (Drini, Mat, Dures, Shkumbin and Vjosa) as well as the Vardar and the Buyukmenderes, produce
 546 positive anomalies in EHOL in winter, due to enhanced winter land precipitation in this simulation
 547 (Figure 10 b and d). The Black Sea net freshwater supply also changes in EHOL with important
 548 decreases in January, February, March and July, but increase in April. In EHOL, the supplementary
 549 winter freshwater input is less pronounced for the western basin than for the eastern basin (Figure 11b),
 550 but major rivers, such as Rhone and Ebro, do show a strong seasonal cycle. As a whole the western basin
 551 sees an increase of river discharges from March to June.

552 In terms of areal means for the entire Mediterranean draining basin, the different components of the
 553 freshwater budget are shown in Table 1 (bottom) for both PICTRL and EHOL, to be compared to the
 554 observation-based estimation OBS and the historical simulation HIST. From PICTRL to EHOL, the
 555 annual precipitation over the Mediterranean Sea itself does not change much, but the annual evaporation
 556 amount shows a slight increase (from 1031 to 1094 mm.year⁻¹). However, the most remarkable feature

557 is the increase of river discharges: 98 mm.year⁻¹ in PICTRL to 225 mm.year⁻¹ in EHOL. The total water
 558 deficit finally decreases from 378 to 305 mm.year⁻¹.

559
 560
 561
 562



563
 564 **Figure 11: Monthly anomalies (EHOL – PICTRL, with seasonal variation) of fresh water**
 565 **discharges (m³.s⁻¹) for major rivers flowing into the western basin (left panel) and the eastern**
 566 **basin (right panel). The sum of all rivers for each basin is also plotted. The Nile and the Black Sea**
 567 **are also shown as rivers of the eastern basin, but not accounted into the basin-scale sum.**

568
 569

570 4.5 Changes in water properties of the Mediterranean Sea

571 At the end of our modelling chain, changes in the properties of the Mediterranean seawater produced by
 572 NEMOMED8 for PICTRL and EHOL are examined. It is important to mention at this stage, that for the
 573 correction of the river runoff the reference is the pre-industrial state, and not the historical simulation
 574 (as is the case for SST and SIC). Our aim was to keep river runoff anomalies free of anthropogenic
 575 influence. In addition, the fact that the “pre-industrial” Nile river runoff (in other words before
 576 damming) is well known influenced this choice. Figure 12 shows changes (EHOL minus PICTRL) for
 577 sea surface salinities, index of stratification and MLD for the last 30 years of simulation. The EHOL
 578 simulation reasonably reaches the steady state in terms of IS, ZOF and SSS, as shown in Figures S6 to
 579 S8 of the supplementary material. The freshwater inputs from the Nile and the north-eastern margin

580 imply a lower salinity in the eastern basin. This decrease in salinity enhances stratification throughout
581 the Mediterranean Sea (with the exception of the Sicily Sea) and affects the convection areas by
582 decreasing the MLD, especially in the Gulf of Lions, in the Adriatic and Ionian Seas and in the Aegean.
583 Such a situation is expected and consistent with the basic climatology of MLD, shown in Figure 5. This
584 global stratification in EHOL is followed by a general reduction in the thermohaline circulation
585 compared to PICTRL (ZOF and MOF, Figure 13).

586

587 Numerous studies have documented the sapropel event S1 and the state of the Mediterranean Sea that
588 caused it. Emeis et al. (2000) mentioned a decreased SSS during this period in both the eastern and
589 western basins (as did Kallel et al., 1997 in the Tyrrhenian basin). In the subsection “*Sea Surface*
590 *Temperatures*” and “*Sea Surface Salinity*” of the section “Text S3” in the supplementary online material,
591 simulated SST and SSS to reconstructions are compared. Although simulated SST is in good agreement
592 with the reconstructed data, there is a gap between the simulated SSS and reconstructions. This
593 discrepancy is not surprising. Indeed, there are many explanations for the underestimation in our model
594 of the salinity. One of them is a common weakness in Early to Mid-Holocene simulations, namely, the
595 underestimation of the northward spread of the African monsoon and therefore, the underestimation of
596 the freshwater flow from North Africa. Adloff (2011), already pointed to a shortfall in freshwater input
597 to reconcile the simulated and observed SSS during the Early Holocene. Our oceanic simulation depicts
598 these behaviours well and is overall similar to previous modelling studies with lower resolution (Adloff
599 et al., 2011; Bosmans et al., 2015; Myers et al., 1998).

600

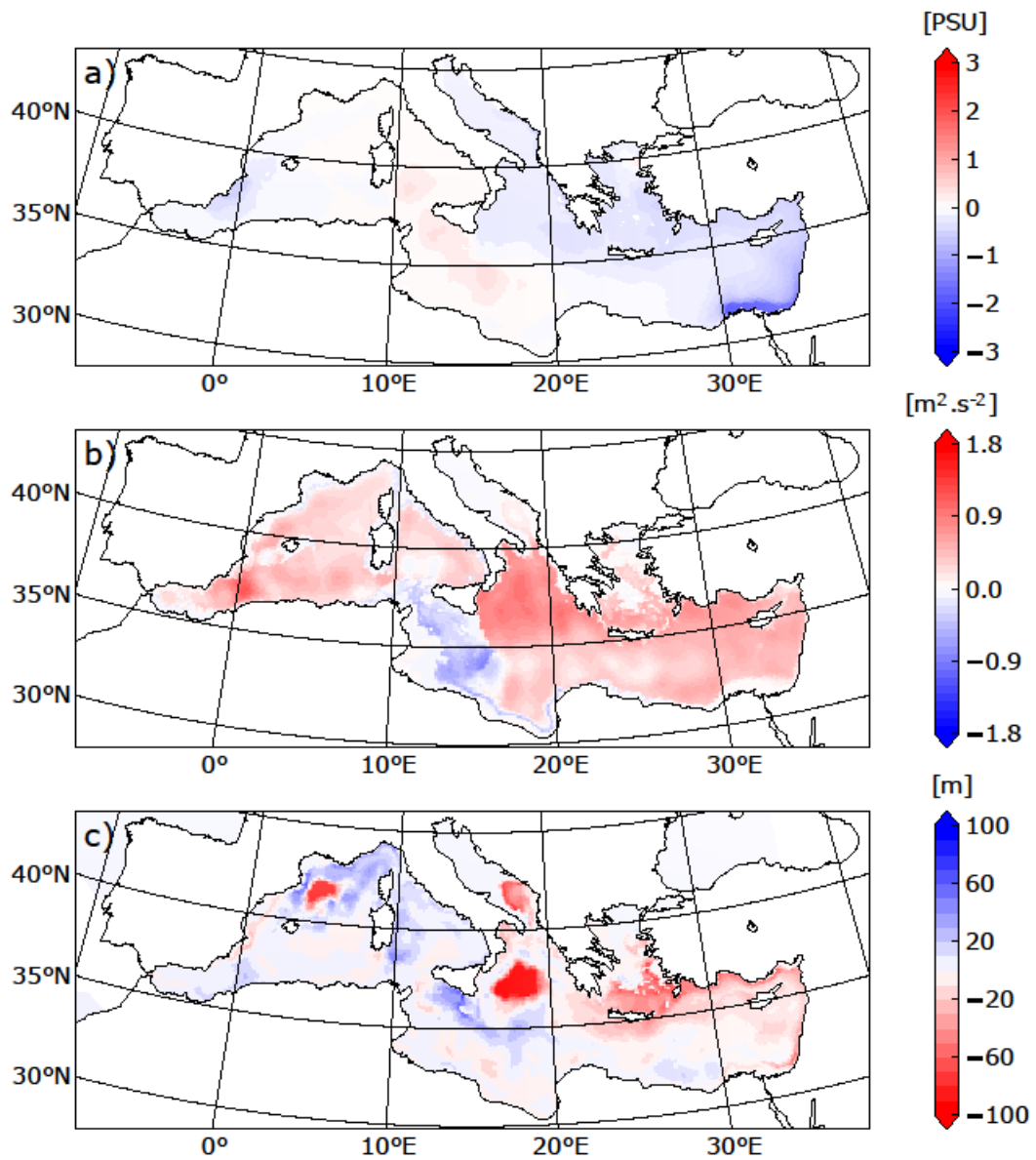
601 Two other issues need to be discussed for the Early Holocene. The first one is sea level, which was 20
602 metres lower than the present day (Peltier et al., 2015). For the sake of simplicity, this difference of sea
603 level is not taken into account in the EHOL simulation. The second issue is the timing of the
604 (re)connection between the Black Sea and the Aegean Sea. This topic is still being debated. Sperling et
605 al. (2003) suggested this reconnection occurred around 8.4 ka BP, while by the calculations of Soulet et
606 al. (2011) it happened around 9 ka BP. Other studies found that an overflow from the Black Sea likely
607 occurred before this reconnection due to Fennoscandian ice-sheet melting during the deglaciation
608 (Chepalyga, 2007; Major et al., 2002; Soulet et al., 2011). For the purposes of this work, the Bosphorus
609 is maintained open in EHOL simulation, with the water exchange set at its modern value.

610

611

612

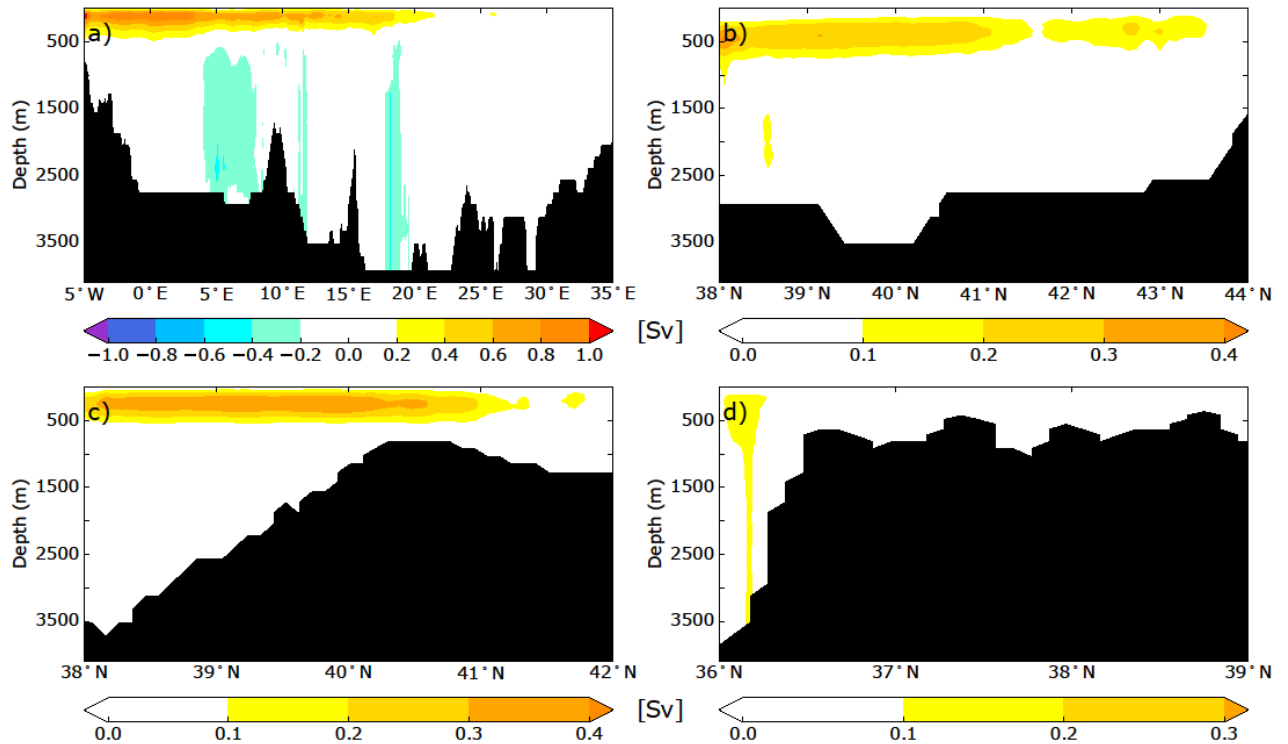
613



614

615 **Figure 12: Deviations between EHOL and PICTRL in a) sea surface salinity, b) index of**

616 **stratification, c) mixed-layer depth, averaged over the last 30 years of simulation**



617
 618 **Figure 13: ZOF (a) and MOF (b, Gulf of Lion, c, Adriatic/Ionian Sea, d, Aegean Sea) for EHOL**
 619 **experiment, averaged over the last 30 years of simulation. These overturning stream-functions**
 620 **were calculated in the same way as in Fig. 6, providing a strict comparison with the experiments**
 621 **HIST and PICTRL.**

622 5 Conclusion and perspectives for the modelling platform

623
 624 This study aimed to develop a modelling platform to simulate different climatic conditions of the
 625 Mediterranean basin. We developed a useful regional climate investigation platform with high spatial
 626 resolution over the Mediterranean region. This is particularly relevant for the study of impacts on the
 627 circulation of the Mediterranean Sea. The model chain has been evaluated for the historical period. We
 628 have presented Early Holocene simulations as an example of the potential of this platform to simulate
 629 past climate. For the Early Holocene, our model reproduced satisfactorily the global and regional climate
 630 features, compared to the observed data. Our platform allowed, for the first time, the generation of a
 631 high-resolution freshwater budget for this period, with a particular focus on continental precipitation, a
 632 key factor for the Mediterranean Sea in the assessment of its impact on circulation during the onset of
 633 the sapropel event, S1. An important limitation of our sequential approach is the fact that it does not
 634 take account of feedback of ocean changes on atmospheric circulation. However, this architecture allows
 635 eventual bias correction, conducted at different levels of the platform if needed. One way to overcome

636 this problem of interactive ocean would be to consider an “asynchronous mode”, namely, to take account
637 of feedback from the ocean component to the atmosphere at a yearly or decadal frequency.

638

639

640 The modelling sequence, moving from global simulation at low resolution to high-resolution regional
641 ocean modelling, avoids the problem of boundary conditions, and provides a fully consistent platform
642 that may be used for many paleoclimate studies. We focused here on the Early Holocene period but this
643 architecture could be used to study other periods investigated in MIPs, such as the Last Glacial
644 Maximum or the deposition of older sapropels, from the Pliocene to the Quaternary, as long as the
645 tectonics remain mainly unchanged (PMIP, PlioMIP).

646

647

648 **Code and data availability.** The current version of LMDZ and NEMO are available from the project
649 website: https://forge.ipsl.jussieu.fr/igcmg_doc/wiki/DocImodelBlmdz and
650 <http://forge.ipsl.jussieu.fr/nemo/wiki/Users> under the terms of the CeCill license for LMDZ and
651 NEMO both. The exact version of the model used to produce the results used in this paper is archived
652 on Zenodo (Vadsaria et al., 2019), as are input data and scripts to run the model and produce the plots
653 for all the simulations presented in this paper.

654

655 **Author’s contribution.** This study was co-designed and approved by all co-authors. The simulation
656 protocol was constructed by TV and LL from a modelling architecture provided by LL. TV conducted
657 the numerical simulations and drafted the first version of the manuscript. All co-authors are largely
658 involved in the writing and revision of the manuscript.

659

660 **Acknowledgments.** We thank Mary Minnock for her professional English revision. This work was
661 supported by the French National program LEFE “HoMoSapiENS”. This work was granted access to
662 the HPC resources of TGCC under the allocation 2017-A0010102212, 2018-A0030102212 and 2018-
663 A004-01-00239 made by GENCI.

664

665

666 **References**

667

668 Adamson, D. A., Gasse, F., Street, F. A. and Williams, M. A. J.: Late Quaternary history of the Nile,
669 Nature, 288(5786), 50–55, doi:10.1038/288050a0, 1980.

670

671 Adler, R., Sapiano, M., Huffman, G., Wang, J.-J., Gu, G., Bolvin, D., Chiu, L., Schneider, U., Becker,
672 A., Nelkin, E., Xie, P., Ferraro, R. and Shin, D.-B.: The Global Precipitation Climatology Project
673 (GPCP) Monthly Analysis (New Version 2.3) and a Review of 2017 Global Precipitation, Atmosphere
674 (Basel), 9(4), 138, doi:10.3390/atmos9040138, 2018.

675

676 Adloff, F., Mikolajewicz, U., Kučera, M., Grimm, R., Maier-Reimer, E., Schmiedl, G. and Emeis, K.-
677 C.: Upper ocean climate of the Eastern Mediterranean Sea during the Holocene Insolation Maximum –
678 a model study" published in *Clim. Past*, 7, 1103–1122, 2011, *Clim. Past*, 7(4), 1149–1168,
679 doi:10.5194/cp-7-1149-2011, 2011.

680

681 Adloff, F., Somot, S., Sevault, F., Jordà, G., Aznar, R., Déqué, M., Herrmann, M., Marcos, M., Dubois,
682 C., Padorno, E., Alvarez-Fanjul, E. and Gomis, D.: Mediterranean Sea response to climate change in an
683 ensemble of twenty first century scenarios, *Clim. Dyn.*, 45(9–10), 2775–2802, doi:10.1007/s00382-015-
684 2507-3, 2015.

685

686 Artale, V.: Role of surface fluxes in ocean general circulation models using satellite sea surface
687 temperature: Validation of and sensitivity to the forcing frequency of the Mediterranean thermohaline
688 circulation, *J. Geophys. Res.*, 107(C8), 3120, doi:10.1029/2000JC000452, 2002.

689

690 Artale, V., Calmanti, S., Carillo, A., Dell’Aquila, A., Herrmann, M., Pisacane, G., Ruti, P. M., Sannino,
691 G., Struglia, M. V., Giorgi, F., Bi, X., Pal, J. S. and Rauscher, S.: An atmosphere–ocean regional climate
692 model for the Mediterranean area: assessment of a present climate simulation, *Clim. Dyn.*, 35(5), 721–
693 740, doi:10.1007/s00382-009-0691-8, 2010.

694

695 Béranger, K., Drillet, Y., Houssais, M.-N., Testor, P., Bourdallé-Badie, R., Alhammoud, B., Bozec, A.,
696 Mortier, L., Bouruet-Aubertot, P. and Crépon, M.: Impact of the spatial distribution of the atmospheric
697 forcing on water mass formation in the Mediterranean Sea, *J. Geophys. Res.*, 115(C12), C12041,
698 doi:10.1029/2009JC005648, 2010.

699

700 Beuvier, J., Sevault, F., Herrmann, M., Kontoyiannis, H., Ludwig, W., Rixen, M., Stanev, E., Béranger,
701 K. and Somot, S.: Modeling the Mediterranean Sea interannual variability during 1961–2000: Focus on
702 the Eastern Mediterranean Transient, *J. Geophys. Res.*, 115(C8), C08017, doi:10.1029/2009JC005950,
703 2010.

704

705 Bosmans, J. H. C., Drijfhout, S. S., Tuenter, E., Lourens, L. J., Hilgen, F. J. and Weber, S. L.: Monsoonal
706 response to mid-holocene orbital forcing in a high resolution GCM, *Clim. Past*, 8(2), 723–740,
707 doi:10.5194/cp-8-723-2012, 2012.

708

709 Bosmans, J. H. C., Drijfhout, S. S., Tuenter, E., Hilgen, F. J., Lourens, L. J. and Rohling, E. J.: Precession
710 and obliquity forcing of the freshwater budget over the Mediterranean, *Quat. Sci. Rev.*, 123, 16–30,
711 doi:10.1016/j.quascirev.2015.06.008, 2015.

712

713 Braconnot, P., Otto-Bliesner, B., Harrison, S., Joussaume, S., Peterchmitt, J., Abe-Ouchi, A., Crucifix,
714 M., Driesschaert, E., Fichefet, T., Hewitt, C. D., Kageyama, M., Kitoh, A., Lâiné, A., Loutre, M., Marti,
715 O., Merkel, U., Ramstein, G., Valdes, P., Weber, S. L., Yu, Y. and Zhao, Y.: Results of PMIP2 coupled
716 simulations of the Mid-Holocene and Last Glacial Maximum – Part 1: experiments and
717 large-scale features, *Clim. Past*, 3(2), 261–277, doi:10.5194/cp-3-261-2007, 2007.

718

719 Callot, Y. and Fontugne, M.: Les étagements de nappes dans les paléolacs holocènes du nord-est du
720 Grand Erg Occidental (Algérie)., 1992.

721

722 Chen, J., Brissette, F. P. and Leconte, R.: Uncertainty of downscaling method in quantifying the impact
723 of climate change on hydrology, *J. Hydrol.*, 401(3–4), 190–202, doi:10.1016/j.jhydrol.2011.02.020,
724 2011.

725

726 Chepalyga, A. L.: The late glacial great flood in the Ponto-Caspian basin, in *The Black Sea Flood*
727 *Question: Changes in Coastline, Climate, and Human Settlement*, pp. 119–148, Springer Netherlands.,
728 2007.

729

730 Dee, D. P., Uppala, S. M., Simmons, A. J., Berrisford, P., Poli, P., Kobayashi, S., Andrae, U.,
731 Balmaseda, M. A., Balsamo, G., Bauer, P., Bechtold, P., Beljaars, A. C. M., van de Berg, L., Bidlot, J.,
732 Bormann, N., Delsol, C., Dragani, R., Fuentes, M., Geer, A. J., Haimberger, L., Healy, S. B., Hersbach,
733 H., Hólm, E. V., Isaksen, L., Kållberg, P., Köhler, M., Matricardi, M., McNally, A. P., Monge-Sanz, B.
734 M., Morcrette, J.-J., Park, B.-K., Peubey, C., de Rosnay, P., Tavolato, C., Thépaut, J.-N. and Vitart, F.:
735 The ERA-Interim reanalysis: configuration and performance of the data assimilation system, *Q. J. R.*
736 *Meteorol. Soc.*, 137(656), 553–597, doi:10.1002/qj.828, 2011.

737

738 Dell’Aquila, A., Calmanti, S., Ruti, P., Struglia, M., Pisacane, G., Carillo, A. and Sannino, G.: Effects
739 of seasonal cycle fluctuations in an A1B scenario over the Euro-Mediterranean region, *Clim. Res.*, 52(1),
740 135–157, doi:10.3354/cr01037, 2012.

741

742 Drobinski, P., Anav, A., Lebeaupin Brossier, C., Samson, G., Stéfanon, M., Bastin, S., Baklouti, M.,
743 Béranger, K., Beuvier, J., Bourdallé-Badie, R., Coquart, L., D’Andrea, F., de Noblet-Ducoudré, N.,
744 Diaz, F., Dutay, J.-C., Ethe, C., Foujols, M.-A., Khvorostyanov, D., Madec, G., Mancip, M., Masson,

745 S., Menut, L., Palmieri, J., Polcher, J., Turquety, S., Valcke, S. and Viovy, N.: Model of the Regional
746 Coupled Earth system (MORCE): Application to process and climate studies in vulnerable regions,
747 *Environ. Model. Softw.*, 35, 1–18, doi:10.1016/j.envsoft.2012.01.017, 2012.

748

749 Dufresne, J.-L., Foujols, M.-A., Denvil, S., Caubel, A., Marti, O., Aumont, O., Balkanski, Y., Bekki, S.,
750 Bellenger, H., Benshila, R., Bony, S., Bopp, L., Braconnot, P., Brockmann, P., Cadule, P., Cheruy, F.,
751 Codron, F., Cozic, A., Cugnet, D., de Noblet, N., Duvel, J.-P., Ethé, C., Fairhead, L., Fichefet, T.,
752 Flavoni, S., Friedlingstein, P., Grandpeix, J.-Y., Guez, L., Guilyardi, E., Hauglustaine, D., Hourdin, F.,
753 Idelkadi, A., Ghattas, J., Joussaume, S., Kageyama, M., Krinner, G., Labetoulle, S., Lahellec, A.,
754 Lefebvre, M.-P., Lefevre, F., Levy, C., Li, Z. X., Lloyd, J., Lott, F., Madec, G., Mancip, M., Marchand,
755 M., Masson, S., Meurdesoif, Y., Mignot, J., Musat, I., Parouty, S., Polcher, J., Rio, C., Schulz, M.,
756 Swingedouw, D., Szopa, S., Talandier, C., Terray, P., Viovy, N. and Vuichard, N.: Climate change
757 projections using the IPSL-CM5 Earth System Model: from CMIP3 to CMIP5, *Clim. Dyn.*, 40(9–10),
758 2123–2165, doi:10.1007/s00382-012-1636-1, 2013.

759

760 Emeis, K.-C., Struck, U., Schulz, H.-M., Rosenberg, R., Bernasconi, S., Erlenkeuser, H., Sakamoto, T.
761 and Martinez-Ruiz, F.: Temperature and salinity variations of Mediterranean Sea surface waters over
762 the last 16,000 years from records of planktonic stable oxygen isotopes and alkenone unsaturation ratios,
763 *Palaeogeogr. Palaeoclimatol. Palaeoecol.*, 158(3–4), 259–280, doi:10.1016/S0031-0182(00)00053-5,
764 2000.

765

766 Fontes, J. C. and Gasse, F.: PALHYDAF (Palaeohydrology in Africa) program: objectives, methods,
767 major results, *Palaeogeogr. Palaeoclimatol. Palaeoecol.*, 84(1–4), 191–215, doi:10.1016/0031-
768 0182(91)90044-R, 1991.

769 Gaven, C., Hillaire-Marcel, C. and Petit-Maire, N.: A Pleistocene lacustrine episode in southeastern
770 Libya, *Nature*, 290(5802), 131–133, doi:10.1038/290131a0, 1981.

771

772 Giorgi, F.: Climate change hot-spots, *Geophys. Res. Lett.*, 33(8), L08707, doi:10.1029/2006GL025734,
773 2006.

774

775 Goubanova, K. and Li, L.: Extremes in temperature and precipitation around the Mediterranean basin
776 in an ensemble of future climate scenario simulations, *Glob. Planet. Change*, 57(1–2), 27–42,
777 doi:10.1016/j.gloplacha.2006.11.012, 2007.

778

779 Harrison, S. P., Bartlein, P. J., Brewer, S., Prentice, I. C., Boyd, M., Hessler, I., Holmgren, K., Izumi,
780 K. and Willis, K.: Climate model benchmarking with glacial and mid-Holocene climates, *Clim. Dyn.*,
781 43(3–4), 671–688, doi:10.1007/s00382-013-1922-6, 2014.

782
783
784
785
786
787
788
789
790
791
792
793
794
795
796
797
798
799
800
801
802
803
804
805
806
807
808
809
810
811
812
813
814
815
816
817
818

Hernández-Díaz, L., Laprise, R., Nikiéma, O. and Winger, K.: 3-Step dynamical downscaling with empirical correction of sea-surface conditions: application to a CORDEX Africa simulation, *Clim. Dyn.*, 48(7–8), 2215–2233, doi:10.1007/s00382-016-3201-9, 2017.

Herrmann, M., Sevault, F., Beuvier, J. and Somot, S.: What induced the exceptional 2005 convection event in the northwestern Mediterranean basin? Answers from a modeling study, *J. Geophys. Res.*, 115(C12), C12051, doi:10.1029/2010JC006162, 2010.

Houpert, L., Testor, P., Durrieu de Madron, X., Somot, S., D’Ortenzio, F., Estournel, C. and Lavigne, H.: Seasonal cycle of the mixed layer, the seasonal thermocline and the upper-ocean heat storage rate in the Mediterranean Sea derived from observations, *Prog. Oceanogr.*, 132, 333–352, doi:10.1016/j.pocean.2014.11.004, 2015.

Hourdin, F., Musat, I., Bony, S., Braconnot, P., Codron, F., Dufresne, J.-L., Fairhead, L., Filiberti, M.-A., Friedlingstein, P., Grandpeix, J.-Y., Krinner, G., LeVan, P., Li, Z.-X. and Lott, F.: The LMDZ4 general circulation model: climate performance and sensitivity to parametrized physics with emphasis on tropical convection, *Clim. Dyn.*, 27(7–8), 787–813, doi:10.1007/s00382-006-0158-0, 2006.

Jalut, G., Dedoubat, J. J., Fontugne, M. and Otto, T.: Holocene circum-Mediterranean vegetation changes: Climate forcing and human impact, *Quat. Int.*, 200(1–2), 4–18, doi:10.1016/j.quaint.2008.03.012, 2009.

Jost, A., Lunt, D., Kageyama, M., Abe-Ouchi, A., Peyron, O., Valdes, P. J. and Ramstein, G.: High-resolution simulations of the last glacial maximum climate over Europe: a solution to discrepancies with continental palaeoclimatic reconstructions?, *Clim. Dyn.*, 24(6), 577–590, doi:10.1007/s00382-005-0009-4, 2005.

Kageyama, M., Braconnot, P., Bopp, L., Caubel, A., Foujols, M.-A., Guilyardi, E., Khodri, M., Lloyd, J., Lombard, F., Mariotti, V., Marti, O., Roy, T. and Woillez, M.-N.: Mid-Holocene and Last Glacial Maximum climate simulations with the IPSL model—part I: comparing IPSL_CM5A to IPSL_CM4, *Clim. Dyn.*, 40(9–10), 2447–2468, doi:10.1007/s00382-012-1488-8, 2013.

Kallel, N., Paterne, M., Labeyrie, L., Duplessy, J.-C. and Arnold, M.: Temperature and salinity records of the Tyrrhenian Sea during the last 18,000 years, *Palaeogeogr. Palaeoclimatol. Palaeoecol.*, 135(1–4), 97–108, doi:10.1016/S0031-0182(97)00021-7, 1997.

819 Kourafalou, V. H. and Barbopoulos, K.: High resolution simulations on the North Aegean Sea seasonal
820 circulation, *Ann. Geophys.*, 21(1), 251–265, doi:10.5194/angeo-21-251-2003, 2003.

821

822 Krinner, G., Viovy, N., de Noblet-Ducoudré, N., Ogée, J., Polcher, J., Friedlingstein, P., Ciais, P., Sitch,
823 S. and Prentice, I. C.: A dynamic global vegetation model for studies of the coupled atmosphere-
824 biosphere system, *Global Biogeochem. Cycles*, 19(1), 1–33, doi:10.1029/2003GB002199, 2005.

825

826 Krinner, G., Llargeron, C., Ménégoz, M., Agosta, C. and Brutel-Vuilmet, C.: Oceanic Forcing of
827 Antarctic Climate Change: A Study Using a Stretched-Grid Atmospheric General Circulation Model, *J.*
828 *Clim.*, 27(15), 5786–5800, doi:10.1175/JCLI-D-13-00367.1, 2014.

829

830 Krinner, G., Beaumet, J., Favier, V., Déqué, M. and Brutel-Vuilmet, C.: Empirical Run-Time Bias
831 Correction for Antarctic Regional Climate Projections With a Stretched-Grid AGCM, *J. Adv. Model.*
832 *Earth Syst.*, 11(1), 64–82, doi:10.1029/2018MS001438, 2019.

833

834 Lacombe, H. and Tchernia, P.: Caractères hydrologiques et circulation des eaux en Méditerranée., in *The*
835 *Mediterranean Sea: A natural sedimentation laboratory*, edited by D. . Stanley, pp. 25–36, Dowden,
836 Hutchinson & Ross, Stroudsburg., 1972.

837

838 De Lange, G. J., Thomson, J., Reitz, A., Slomp, C. P., Speranza Principato, M., Erba, E. and Corselli,
839 C.: Synchronous basin-wide formation and redox-controlled preservation of a Mediterranean sapropel,
840 *Nat. Geosci.*, 1(9), 606–610, doi:10.1038/ngeo283, 2008.

841

842 Lebeaupin Brossier, C., Béranger, K., Deltel, C. and Drobinski, P.: The Mediterranean response to
843 different space–time resolution atmospheric forcings using perpetual mode sensitivity simulations,
844 *Ocean Model.*, 36(1–2), 1–25, doi:10.1016/j.ocemod.2010.10.008, 2011.

845

846 Lézine, A.-M. and Casanova, J.: Correlated oceanic and continental records demonstrate past climate
847 and hydrology of North Africa (0-140 ka), *Geology*, 19(4), 307–310, doi:10.1130/0091-
848 7613(1991)019<0307:COACRD>2.3.CO;2, 1991.

849

850 Li, L., Bozec, A., Somot, S., Bouruet-Aubertot, P. and Crepon, M.: Regional atmospheric, marine
851 processes and climate modelling, in *Mediterranean climate variability and predictability*, edited by P.
852 Lionello, P. Malanotte-Rizzoli, and R. Boscolo, Elsevier., 2006.

853

854 Li, L., Casado, A., Congedi, L., Dell’Aquila, A., Dubois, C., Elizalde, A., L’Hévéder, B., Lionello, P.,
855 Sevault, F., Somot, S., Ruti, P. and Zampieri, M.: Modeling of the mediterranean climate system, in *The*

856 Climate of the Mediterranean Region, pp. 419–448, Elsevier Inc., 2012.

857

858 Li, Z.-X.: Ensemble Atmospheric GCM Simulation of Climate Interannual Variability from 1979 to
859 1994, *J. Clim.*, 12(4), 986–1001, doi:10.1175/1520-0442(1999)012<0986:EAGSOC>2.0.CO;2, 1999.

860 Locarnini, R. A., Mishonov, A. V., Antonov, J. I., Boyer, T. P., Garcia, H. E., Baranova, O. K., Zweng,
861 M. M., Paver, C. R., Reagan, J. R., Johnson, D. R., Hamilton, M. and Seidov, D.: World Ocean Atlas
862 2013. Vol. 1: Temperature., S. Levitus, Ed.; A. Mishonov, Tech. Ed.; NOAA Atlas NESDIS,
863 73(September), 40, doi:10.1182/blood-2011-06-357442, 2013.

864

865 Ludwig, P., Shao, Y., Kehl, M. and Weniger, G.-C.: The Last Glacial Maximum and Heinrich event I
866 on the Iberian Peninsula: A regional climate modelling study for understanding human settlement
867 patterns, *Glob. Planet. Change*, 170, 34–47, doi:10.1016/j.gloplacha.2018.08.006, 2018.

868

869 Ludwig, W., Dumont, E., Meybeck, M. and Heussner, S.: River discharges of water and nutrients to the
870 Mediterranean and Black Sea: Major drivers for ecosystem changes during past and future decades?,
871 *Prog. Oceanogr.*, 80(3–4), 199–217, doi:10.1016/j.pocean.2009.02.001, 2009.

872

873 Macias, D. M., Garcia-Goriz, E. and Stips, A.: Productivity changes in the Mediterranean Sea for the
874 twenty-first century in response to changes in the regional atmospheric forcing, *Front. Mar. Sci.*, 2,
875 doi:10.3389/fmars.2015.00079, 2015.

876

877 Madec, G.: NEMO ocean engine-version 3.0-Laboratoire d’Océanographie et du Climat:
878 Expérimentation et Approches Numériques, 2008.

879

880 Magny, M., de Beaulieu, J.-L., Drescher-Schneider, R., Vannièrè, B., Walter-Simonnet, A.-V., Miras,
881 Y., Millet, L., Bossuet, G., Peyron, O., Brugiapaglia, E. and Leroux, A.: Holocene climate changes in
882 the central Mediterranean as recorded by lake-level fluctuations at Lake Accessa (Tuscany, Italy), *Quat.*
883 *Sci. Rev.*, 26(13–14), 1736–1758, doi:10.1016/j.quascirev.2007.04.014, 2007.

884

885 Magny, M., Combourieu-Nebout, N., de Beaulieu, J. L., Bout-Roumazielles, V., Colombaroli, D.,
886 Desprat, S., Francke, A., Joannin, S., Ortu, E., Peyron, O., Revel, M., Sadori, L., Siani, G., Sicre, M. A.,
887 Samartin, S., Simonneau, A., Tinner, W., Vannièrè, B., Wagner, B., Zanchetta, G., Anselmetti, F.,
888 Brugiapaglia, E., Chapron, E., Debret, M., Desmet, M., Didier, J., Essallami, L., Galop, D., Gilli, A.,
889 Haas, J. N., Kallel, N., Millet, L., Stock, A., Turon, J. L. and Wirth, S.: North and south
890 palaeohydrological contrasts in the central Mediterranean during the Holocene: tentative synthesis and
891 working hypotheses, *Clim. Past*, 9(5), 2043–2071, doi:10.5194/cp-9-2043-2013, 2013.

892

893 Major, C., Ryan, W., Lericolais, G. and Hajdas, I.: Constraints on Black Sea outflow to the Sea of
894 Marmara during the last glacial–interglacial transition, *Mar. Geol.*, 190(1–2), 19–34,
895 doi:10.1016/S0025-3227(02)00340-7, 2002.

896

897 Marzin, C. and Braconnot, P.: Variations of Indian and African monsoons induced by insolation changes
898 at 6 and 9.5 kyr BP, *Clim. Dyn.*, 33(2–3), 215–231, doi:10.1007/s00382-009-0538-3, 2009.

899

900 Mikolajewicz, U.: Modeling Mediterranean Ocean climate of the Last Glacial Maximum, *Clim. Past*,
901 7(1), 161–180, doi:10.5194/cp-7-161-2011, 2011.

902

903 Millot, C. and Taupier-Letage, I.: Circulation in the Mediterranean Sea, pp. 29–66., 2005.

904

905 Myers, P. G., Haines, K. and Rohling, E. J.: Modeling the paleocirculation of the Mediterranean: The
906 Last Glacial Maximum and the Holocene with emphasis on the formation of sapropel S 1,
907 *Paleoceanography*, 13(6), 586–606, doi:10.1029/98PA02736, 1998.

908

909 Peltier, W. R., Argus, D. F. and Drummond, R.: Space geodesy constrains ice age terminal deglaciation:
910 The global ICE-6G_C (VM5a) model, *J. Geophys. Res. Solid Earth*, 120(1), 450–487,
911 doi:10.1002/2014JB011176, 2015.

912

913 Petit-Maire, N., Fontugne, M. and Rouland, C.: Atmospheric methane ratio and environmental change
914 in the Sahara an Sahel during the last 130 kyrs, *Palaeogeogr. Palaeoclimatol. Palaeoecol.*, 86(1–2), 197–
915 206, doi:10.1016/0031-0182(91)90009-G, 1991.

916

917 Peyron, O., Goring, S., Dormoy, I., Kotthoff, U., Pross, J., de Beaulieu, J.-L., Drescher-Schneider, R.,
918 Vanni re, B. and Magny, M.: Holocene seasonality changes in the central Mediterranean region
919 reconstructed from the pollen sequences of Lake Accesa (Italy) and Tenaghi Philippon (Greece), *The*
920 *Holocene*, 21(1), 131–146, doi:10.1177/0959683610384162, 2011.

921

922 Pinardi, N., Cessi, P., Borile, F. and Wolfe, C. L. P.: The Mediterranean sea overturning circulation, *J.*
923 *Phys. Oceanogr.*, 49(7), 1699–1721, doi:10.1175/JPO-D-18-0254.1, 2019.

924

925 Ramstein, G., Kageyama, M., Guiot, J., Wu, H., H ely, C., Krinner, G. and Brewer, S.: How cold was
926 Europe at the Last Glacial Maximum? A synthesis of the progress achieved since the first PMIP model-
927 data comparison, *Clim. Past*, 3(2), 331–339, doi:10.5194/cp-3-331-2007, 2007.

928

929 Revel, M., Colin, C., Bernasconi, S., Combourieu-Nebout, N., Ducassou, E., Grousset, F. E., Rolland,

930 Y., Migeon, S., Bosch, D., Brunet, P., Zhao, Y. and Mascle, J.: 21,000 Years of Ethiopian African
931 monsoon variability recorded in sediments of the western Nile deep-sea fan, *Reg. Environ. Chang.*,
932 14(5), 1685–1696, doi:10.1007/s10113-014-0588-x, 2014.

933

934 Rossignol-Strick, M., Nesteroff, W., Olive, P. and Vergnaud-Grazzini, C.: After the deluge:
935 Mediterranean stagnation and sapropel formation, *Nature*, 295(5845), 105–110, doi:10.1038/295105a0,
936 1982.

937

938 Sanchez-Gomez, E., Somot, S., Josey, S. A., Dubois, C., Elguindi, N. and Déqué, M.: Evaluation of
939 Mediterranean Sea water and heat budgets simulated by an ensemble of high resolution regional climate
940 models, *Clim. Dyn.*, 37(9–10), 2067–2086, doi:10.1007/s00382-011-1012-6, 2011.

941

942 Sevault, F., Somot, S., Alias, A., Dubois, C., Lebeaupin-Brossier, C., Nabat, P., Adloff, F., Déqué, M.
943 and Decharme, B.: A fully coupled Mediterranean regional climate system model: design and evaluation
944 of the ocean component for the 1980–2012 period, *Tellus A Dyn. Meteorol. Oceanogr.*, 66(1), 23967,
945 doi:10.3402/tellusa.v66.23967, 2014.

946

947 Somot, S., Sevault, F. and Déqué, M.: Transient climate change scenario simulation of the
948 Mediterranean Sea for the twenty-first century using a high-resolution ocean circulation model, *Clim.*
949 *Dyn.*, 27(7–8), 851–879, doi:10.1007/s00382-006-0167-z, 2006.

950

951 Somot, S., Sevault, F., Déqué, M. and Crépon, M.: 21st century climate change scenario for the
952 Mediterranean using a coupled atmosphere–ocean regional climate model, *Glob. Planet. Change*, 63(2–
953 3), 112–126, doi:10.1016/j.gloplacha.2007.10.003, 2008.

954

955 Soulet, G., Ménot, G., Garreta, V., Rostek, F., Zaragosi, S., Lericolais, G. and Bard, E.: Black Sea
956 “Lake” reservoir age evolution since the Last Glacial — Hydrologic and climatic implications, *Earth*
957 *Planet. Sci. Lett.*, 308(1–2), 245–258, doi:10.1016/j.epsl.2011.06.002, 2011.

958

959 Sperling, M., Schmiedl, G., Hemleben, C., Emeis, K. ., Erlenkeuser, H. and Grootes, P. .: Black Sea
960 impact on the formation of eastern Mediterranean sapropel S1? Evidence from the Marmara Sea,
961 *Palaeogeogr. Palaeoclimatol. Palaeoecol.*, 190, 9–21, doi:10.1016/S0031-0182(02)00596-5, 2003.

962

963 Stanev, E. V., Le Traon, P.-Y. and Peneva, E. L.: Sea level variations and their dependency on
964 meteorological and hydrological forcing: Analysis of altimeter and surface data for the Black Sea, *J.*
965 *Geophys. Res. Ocean.*, 105(C7), 17203–17216, doi:10.1029/1999JC900318, 2000.

966

967 Stickler, A., Brönnimann, S., Valente, M. A., Bethke, J., Sterin, A., Jourdain, S., Roucaute, E., Vasquez,
968 M. V., Reyes, D. A., Allan, R. and Dee, D.: ERA-CLIM: Historical Surface and Upper-Air Data for
969 Future Reanalyses, *Bull. Am. Meteorol. Soc.*, 95(9), 1419–1430, doi:10.1175/BAMS-D-13-00147.1,
970 2014.

971

972 Swingedouw, D., Colin, C., Eynaud, F., Ayache, M. and Zaragosi, S.: Impact of freshwater release in
973 the Mediterranean Sea on the North Atlantic climate, *Clim. Dyn.*, 53(7–8), 3893–3915,
974 doi:10.1007/s00382-019-04758-5, 2019.

975

976 Vadsaria, T., Li, L., Ramstein, G. and Dutay, J.-C.: Model and output for Vadsaria et al, “Development
977 of a sequential tool LMDZ-NEMO-med-V1 for global to regional past climate simulation over the
978 Mediterranean basin: an early Holocene case study”, GMD publication, ,
979 doi:10.5281/ZENODO.3258410, 2019.

980

981 Vorosmarty, C. J., Feteke, B. M. and Tucker, B. A.: Global River Discharge, 1807-1991, V. 1.1
982 (RivDIS), , doi:https://doi.org/10.3334/ORNLDAAC/199, 1998.

983

984 Williams, M.: Late Quaternary environments in the White Nile region, Sudan, *Glob. Planet. Change*,
985 26(1–3), 305–316, doi:10.1016/S0921-8181(00)00047-3, 2000.

986

987 Zanchetta, G., Drysdale, R. N., Hellstrom, J. C., Fallick, A. E., Isola, I., Gagan, M. K. and Pareschi, M.
988 T.: Enhanced rainfall in the Western Mediterranean during deposition of sapropel S1: stalagmite
989 evidence from Corchia cave (Central Italy), *Quat. Sci. Rev.*, 26(3–4), 279–286,
990 doi:10.1016/j.quascirev.2006.12.003, 2007.

991

992 de Zolt, S., Lionello, P. and Malguzzi, P.: Implementation of an aorc in the mediterranean sea, 2003.

993 Zweng, M. M., Reagan, J. R., Antonov, J. I., Mishonov, A. V., Boyer, T. P., Garcia, H. E., Baranova,
994 O. K., Johnson, D. R., Seidov, D. and Bidlle, M. M.: World Ocean Atlas 2013, Volume 2: Salinity,
995 NOAA Atlas NESDIS, 2(1), 39, doi:10.1182/blood-2011-06-357442, 2013.

996

997